UNIVERSITY OF CALIFORNIA,
IRVINE

Automated Detection of Fast Ripples and Rejection of Artifacts in Human Scalp Electroencephalogram

THESIS

Submitted in partial satisfaction of the requirements for the degree of

MASTER OF SCIENCE

in Biomedical Engineering

by

Tian Lan

Thesis Committee:
Assistant Professor Beth Lopour, Chair
Associate Professor Zoran Nenadic
Professor Frithjof Kruggel

2017

Dedication

To

My parents and friends

for their endless love and unconditional support

Table of Contents

LIST OF FIGURES

LIST OF TABLES

ACKNOWLEGMENTS

Firstly, I would like to express my sincere gratitude to my advisor, Prof. Beth Lopour, for her continuous guidance and support during my study at UC Irvine. Since the beginning of my Master's research in the first quarter, she's been both a good mentor and a friend. Her patience, encouragement and inspiration always helped me to tackle challenges during research and guided me to find out the best solution.

Besides my advisor, I want to express my appreciation to my thesis committees, Prof. Zoran Nenadic and Dr. Frithjof Kruggel. Without their support and insightful comments to my thesis, I wouldn't be able to complete my thesis from various perspectives. Also, what they taught me during lectures in previous quarters were priceless treasures which let me make progress and be more confident doing research in this field.

Also, I want to say thank you to Dr. Joyce Wu at UCLA Health. She funded me in Summer 2016 and provided me with a large amount of clinical data. Her suggestions from a doctor's prospective were insightful. All these were helpful to me and the continuous progress of this project.

Appreciation also goes to my lab mates, Krit and Rachel, who always gave me inspirations and help when I was facing obstacles. Their experience in doing research and hospitality in daily life made me feel warm in the lab.

Last but not least, I would like to appreciate my friends for being with me in the past years and always making me feel loved. And of course, I would like to thank my parents for their love and care, without which my Master's research and thesis wouldn't have been possible.

ABSTRACT OF THE THESIS

Automated Detection of Fast Ripples and Rejection of Artifacts in Human Scalp Electroencephalogram

By

Tian Lan

Master of Science in Biomedical Engineering

University of California, Irvine 2017

Assistant Professor Beth Lopour, Chair

High frequency oscillations (HFOs) are a promising biomarker of epileptic tissues. Higher rates of HFOs are observed in seizure onset zones (SOZ) compared to other areas. However, the detection of these events and their relation to epileptogenesis is still challenging because there is no formal or global definition of HFO. Visual annotations of HFOs are regarded as the gold standard, but they are extremely tedious, inevitably subjective and require a large amount of concentration. Some previously published automatic detectors show promising performance, but they usually require the optimization of several parameters and supervised validation. In order to simplify this procedure and implement automatic detection of HFOs broadly in scalp EEG data, we modified an automatic HFO detection algorithm initially designed for intracranial EEG data and adapted it to scalp EEG data. The algorithm is based on the iterative estimation of the amplitude distribution of the

EEG background activity. It requires the optimization of two parameters related to the number of detected events and determines different optimized threshold values for each 1-minute window in each channel using the iterative procedure. Since scalp EEG can be easily influenced by artifacts like muscle movements, sharp waves and fast transients, it is not trivial to remove such artifacts and achieve good performance. Therefore, several post-processing methods were applied to remove spurious detections and reduce the number of false detections. This procedure was completed with the aid of a new interface which provided good visualization of visually marked HFOs and automatically detected events.

After applying the algorithm to an EEG dataset, we examined the distribution of events detected in all channels and found that the detector had much better performance in subjects where HFOs were mainly concentrated in less than five channels and stood out obviously from background activities. Overall, our detector achieved a true positive rate (sensitivity) of 86.3% and false detection rate (FDR) of 11.3%. If better sensitivity was desired, allowing more false detections, the detector provided a TPR of 91.2% and FDR of 31.7%. After doing a leave-one-out cross-validation within all patients, a TPR of 80.4% and FDR of 32.7% were obtained. We consider this algorithm a powerful tool in localizing high frequency epileptic activities in scalp EEG data due to its advantage in high sensitivity, low false detection rate and the implementation of several artifact rejection methods.

Chapter 1 Introduction

1.1 Electroencephalography (EEG)

Electroencephalography (EEG) is an imaging method used to record the potentials reflecting the electrical activity of the brain. The EEG signal is a bioelectrical signal representing the aggregate response of the highly-correlated brain cells in cerebral cortex or thalamus measured on the surface of scalp. Various forms of mental states and pathology in different parts of the cerebral cortex are reflected in different EEG characteristics, therefore the EEG signal contains both physiological and disease information.

EEG measures the voltage fluctuations resulting from post-synaptic currents generated in the human brain. It was hypothesized that the changes in the brain currents depend on the status of the brain, including wakefulness, sleep, coma, anesthesia, epilepsy, *etc*. During an EEG test, electrodes are placed on the scalp surface while connected to an amplifier as well as an EEG recording machine. The signals conducted from different electrodes are then displayed and recorded (Siuly. 2012). The number of electrodes might vary from 1 to 512 depending on the exact application of the EEG recordings. The most commonly used standardized placement of scalp electrodes has been the International 10/20 system, in which the distance in percentages of the 10/20 range between Nasion-Inion and fixed points determines the location of each electrode. Electrodes are marked with regard to their corresponding brain regions, including the Frontal pole (Fp), Central (C), Parietal (P), occipital (O), and Temporal (T), while “z” refers to an electrode placed on the midline. Odd numbers are used as a subscript for points on the brain left hemisphere while

even numbers stand for those on the right hemisphere. An example of standardized 10/20 system is shown in **Figure 1.1.** [https://www.medicine.mcgill.ca/physio/vlab/biomed_signals/eeg_n.htm]

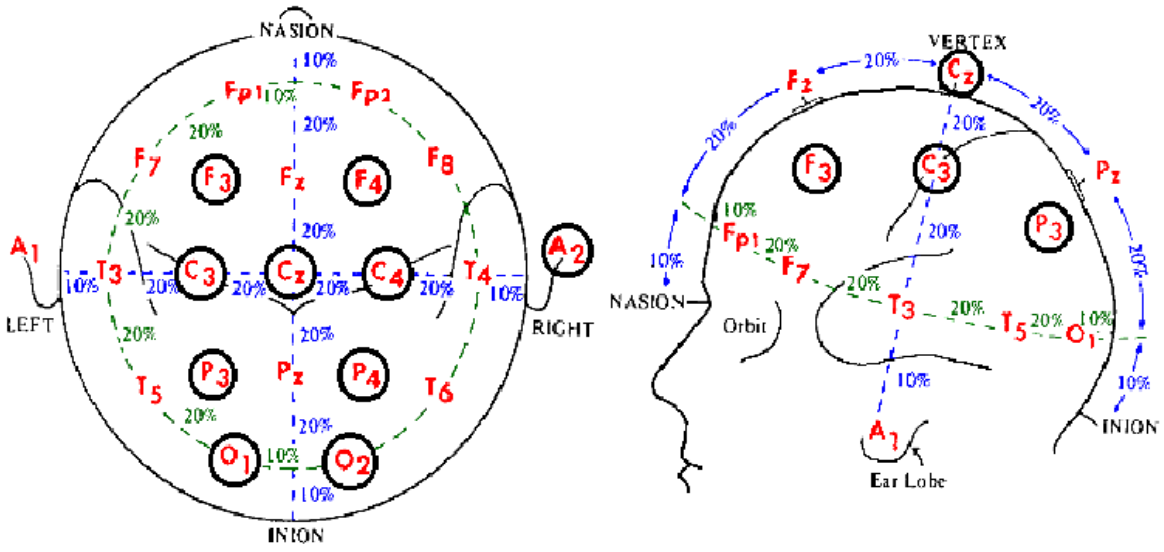

Figure 1.1. A standardized international 10/20 electrode placement system

EEG doesn't record directly the voltage detected at each electrode. Instead, the signal displayed on the screen of the EEG recording machine represents the difference between two electrodes, namely the difference between the active electrode and reference electrode. The way that electrode pairs are arranged, or the placement of electrodes on the scalp, is known as a montage. Recordings of EEG can be viewed under many different preprogrammed montages.

One commonly used montage in EEG recording is the bipolar montage. Instead of using one common reference for all channels, bipolar means that you have two electrodes per one channel, so you have a different reference electrode for each channel. Each recorded

waveform represents the difference between two adjacent electrodes. For example, the channel "Fp1-F7" stands for the difference in the voltage between the Fp1 electrode and the F7 electrode. The next channel in the montage, "F7-T3," represents the voltage difference between F7 and T3. An example of a longitudinal bipolar montage is shown in **Figure 1.2.** [http://aibolita.com/nervous-diseases/3055-montage-selection.html]

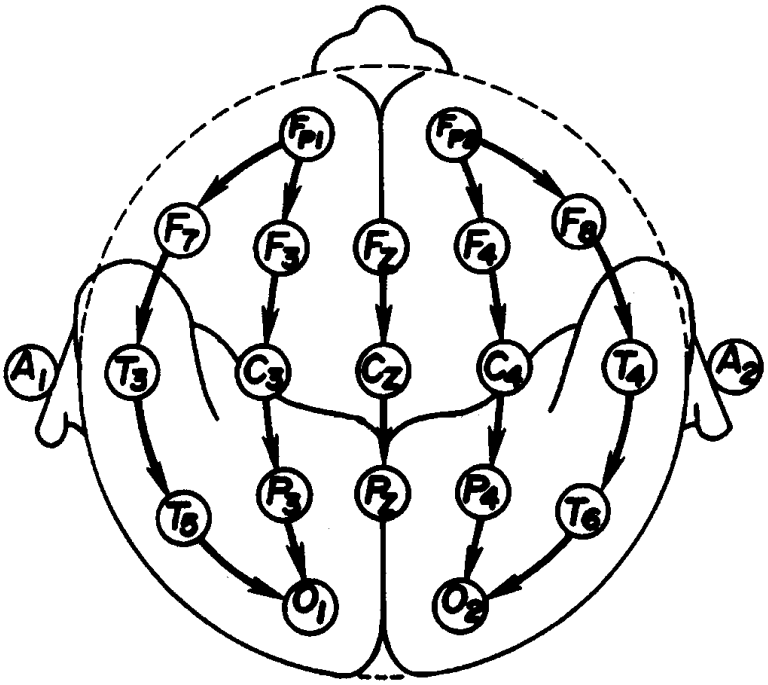

Figure 1.2. Example of a longitudinal bipolar montage

1.2 EEG rhythms and high frequency oscillations

EEG waveforms are commonly classified according to their frequency and spatial distribution. Healthy EEG signals consist of a wide range of frequencies. Features specific to certain frequencies are very important when assessing abnormalities in EEG and understanding functional behaviors (Siuly. 2012).

Scalp EEG is typically categorized into five frequency bands: delta (0.5-4Hz), theta (4-8Hz), alpha (8-13Hz), beta (13-30Hz) and gamma (>30Hz). Among these five frequency bands, delta waves are slowest in frequency but the highest in amplitude. These oscillations dominate in infants up to one year old and mostly appear in adults during stage 3 and 4 of sleep. Theta waves usually have an amplitude higher than 20 μV and are the dominant rhythm in young children. They also frequently appear in rapid eye movement (REM) sleep in adults. Alpha rhythms are mostly seen with eyes closed or relaxed with a mental awareness. Beta activity is referred to as “fast” activity. It is regarded as a normal rhythm and is dominant when an adult is anxious or alert with his/her eyes open. However, a large amount of beta activities with high amplitude could be a signal of abnormality. The gamma band is linked to peak concentration and the brain’s optimal frequency for cognitive as well as motor functions (Yazdanpour-Naeini et al. 2012).

In addition to these five widely studied frequency bands in human scalp EEG, high frequency oscillations have recently begun receiving wide attention. High frequency oscillations (HFOs) are field potentials that reflect short-term synchronization of neuronal activity (normally less than 100ms) and they generally occur during the non-rapid eye movement (NREM) state. They are spontaneous EEG patterns in the range of 80–500 Hz,

consisting of at least four oscillations that can be “clearly” distinguished from background (Engel et al. 2012). Also, they are believed to play crucial roles in both normal and pathologic brain functions (Engel Jr et al. 2009). There is accumulating evidence that an increased rate of HFOs is associated with the seizure onset zone (Bragin A et al. 1999) and that resection of HFO-generating tissue is correlated to seizure-free outcomes (Jacobs J et al. 2010, Wu et al. 2010). In general, high frequency oscillations (HFO) are a promising biomarker for localization of epileptogenic tissues (Bragin A et al. 2000). However, there is a need to improve the understanding of pathophysiology of epilepsy, delineate the seizure onset zones in epileptic patients, and bring about predictions of surgical outcomes using high frequency activity.

HFOs are broadly classified into ripples and fast ripples (FR) and range between 80-250 Hz and 250-500 Hz, respectively. Ripples have been seen in both humans and rodents, where they are associated with epileptic processes. Fast ripples were first recorded in rodents from hippocampus and entorhinal cortex during interictal periods (Bragin et al. 1999). Although fast ripples and ripples are closely related due to the fact that they both are strongly expressed in slow wave sleep, fast ripples can be clearly distinguished because they also appear in dentate gyrus, a place where no ripples are seen (Jasper. 2012). It should be noted that in the identification of seizure onset zones, fast ripples were demonstrated to be more specific and accurate (Urrestarazu et al. 2007). Also, it was found that the removal of brain areas exhibiting fast ripples was associated with better clinical outcomes (Akiyama et al. 2011, Wu et al. 2010, van Klink et al. 2014).

Researchers have been primarily studying fast oscillations and high frequency oscillations in intracranial EEG data. However, Zelmann *et al* stated in 2014 that HFOs were also visible in human scalp EEG and could become powerful biomarkers of epileptogenicity (Zelmann et al., 2014). This brought about a possibility that automatic detection of HFOs might also be applied to human scalp EEG data. There are other published studies using scalp EEG data (Wu et al. 2008., Andrade-Valenca et al., 2011, Cosandier-Rimélé et al., 2011. Iwatani et al., 2012, Melani et al., 2013, Zelmann et al., 2014, von Ellenrieder et al., 2014, Kobayashi et al., 2014, Pizzo et al., 2016). Some groups have suggested that high epileptic fast oscillation rates in hypsarrhythmia (40~150 Hz) are associated with the process of pathological neurodevelopment in West syndrome (Iwatani et al., 2012, Kobayashi et al., 2014). Interictal fast oscillations were specific in identifying children with epilepsy (Wu et al., 2008) and localizing the seizure onset zone (Andrade-Valenca et al., 2011). Although many researchers have studied high frequency oscillations measured from human scalp EEG data while indicating promising clinical outcomes, there is still a need for the development of automatic detection of HFOs, especially for fast ripple events.

1.3 Previous studies of automatic detection of HFOs in human subjects

HFO detection has been historically performed by visual review of the electrophysiological data. Human annotations are still considered the gold standard for HFO identification. However, despite its valuable advantage of providing an advanced understanding of the relationship between HFOs and epileptogenesis, the detection of high frequency activity with manual processing is highly time-consuming, complicated (López-Cuevas et al. 2013) and subjective. Discrepancies between human reviewers can reach up to

40% (Gardner et al. 2007) and visual processing of a 10-channel, 10-min dataset can take up to ten hours while requiring large amount of concentration. To overcome these shortcomings, many automatic HFO detectors have been developed in the recent years based on different detection schemes. One of the common goals of these detectors is to improve the accuracy and precision of HFO detection while shortening processing time (Chaibi et al. 2013).

A number of automatic detectors have been created for use on ECoG data. In 2002, Staba *et al.* developed a detector based on the energy, defined as the moving average of the root mean square amplitude of a filtered signal. This detector provided a sensitivity of 84% and false detections were rejected based on the event duration and number of oscillations (Staba et al. 2002). The detector proposed by Gardner *et al*. in 2007 detected events from the background signal using frequency equalization / line-length energy, and a sensitivity of 89.5% was reported (Gardner et al. 2007). Then in 2010, Crépon *et al*. proposed a detector based on the Hilbert envelope and reported a good sensitivity (100%) as well as the first report of specificity (91%). Similar to the Hilbert detector in removing false positives by looking at event duration, Zelmann *et al*. developed a detector in 2012 making use of wavelet entropy and RMS amplitude and applied it to ECoG signals in 80-450 Hz. Other than these, there were published detectors applying techniques including tunable Q-factor wavelet transform in conjunction with morphological component analysis (MCA) and local maxima in the normalized time-frequency transform (Morlet Wavelet) (Chaibi et al. 2014), power estimation by multitaper method/power peak detection (Wang J et al. 2014), and baseline detection by wavelet entropy Hilbert envelope (Fedele et al. 2016). The false detection rejection methods in these detectors are based on the application of time-frequency analysis

using Stockwell Transform and morphologic characterization of events in frequency (Burnos et al. 2014), spatial mapping (Wang J et al. 2014) and multichannel spatial information computing correlation of distant electrodes (Fedele et al. 2016). Automatic detection of fast oscillations (40~200 Hz) in human scalp EEG proposed by von Ellenrieder *et al* in 2011 applied RMS amplitudes with adaptive window sizes and thresholding according to the frequency sub-band in the detection procedure, while relying on the optimization of threshold value by expert annotations in false events' rejection (von Ellenrieder et al. 2011).

1.4 Motivation of this project

Currently, the automatic detection of HFO events typically consists of the initial detection of candidate events and the rejection of artifacts and false detections. Most of the published algorithms are adapted to invasively recorded ECoG data and are well-suited. However, some of these published detectors accept the results without applying any post-processing methods, while some others increase the complexity of the algorithm through the optimization of several parameters, rendering them overparameterized. Although they obtain good sensitivity, it makes implementation much more complicated and difficult. Also, a large number of detectors require human visual validation for the rejection of artifacts and false positives after the detection procedure, which makes the entire detection semi-supervised.

Therefore, there is a need to design an automatic detector of HFOs for use on scalp EEG data. It should have a simple parameter optimization procedure and implement post-processing steps, such as artifact rejection, without any supervised procedures. This will aid

in the broad application of automatic detection of HFOs in scalp EEG data and the translation of automated HFO detection to clinical settings.

Here, we propose a new algorithm for the automatic detection of HFOs in human scalp EEG data based on an existing algorithm designed for human intracranial data (Charupanit et al. 2017). In this method, two parameters need to be optimized to obtain an optimal balance between sensitivity and specificity: the threshold and the number of oscillations. The detection is performed on rectified filtered EEG signals, and an iterative process is used to estimate the probability distribution of background signals based on their amplitude. This enables the selection of an optimal threshold. This algorithm achieves good performance when the results are compared to visual annotations. Also, the implementation of an interface used to localize HFOs in a bipolar montage and several artifact rejection methods offer advantages over alternative methods for the detection of candidate HFO events. The significance of this algorithm is that it makes the automatic detection of fast ripples in human scalp EEG available while providing high sensitivity as well as low false detection rate. Also, the artifact rejection methods applied in the post-processing procedure render the detector highly flexible when it is tested in datasets from different sources.

Chapter 2 Methods

2.1 EEG recordings and human visual annotations of HFOs

All data used in this research were recorded at UCLA Mattel Children's Hospital as a part of the TACERN (Tuberous Sclerosis Complex Autism Center of Excellence Network) database, which was created to study epilepsy and autism in pediatric patients with Tuberous Sclerosis Complex (TSC). The EEG recordings were collected between 2013 and 2015 under standard 10-20 configuration from seven epilepsy patients suffering from TSC. The seven subjects studied in this project had an average age of 362 days (range 87-531 days). For each patient, 12-minute EEG signals under resting state were recorded. However, the first and last minute of the recordings were removed, leaving the 10-minute recordings in between to be used for HFO visual analysis.

All HFO visual analysis was conducted by two experienced reviewers at UCLA Medical Center. The software used during the visual analysis was Persyst (Persyst Development Corporation, San Diego, CA), an EEG software package using digital signal processing and neural network analysis to remove artifacts and interpret EEG data. During the human annotation, the EEG signal was bandpass filtered into the fast ripple band. The sampling rate for the data was 2000 Hz and each window in the Persyst interface contained 1 second of 18-channel EEG data. A longitudinal bipolar montage was used to re-reference the signal. The interface displaying the environment of HFO visual analysis is shown in **Figure 2.1.**

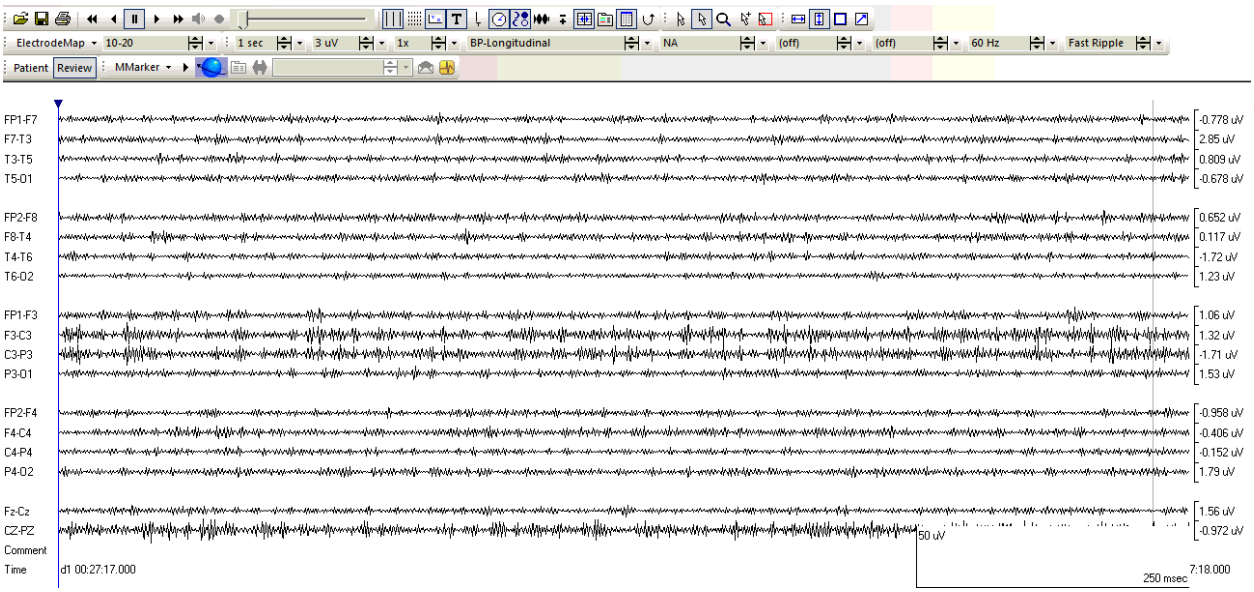

Figure 2.1. Persyst main interface used for HFOs visual annotation

During visual analysis, the duration and location of each HFO event was marked and recorded for future reference. Fast ripples were defined as oscillatory events with at least four cycles and a center frequency occurring between 250-500 Hz. Using the Persyst EEG reviewing software, fast ripple events were marked by human reviewers using a finite-impulse response bandpass filter between 250-500 Hz and EEG visualized with an amplitude scale of 1uV/mm and time scale of 338mm/sec. All EEG raw signals were then exported and saved from Insight III, an affiliated software of Persyst. In addition to the comments on the information of each HFO event, there were also time points showing other annotations made during the EEG recording, such as when the patient smiled, cried and screamed, *etc*.

2.2 Automated detection algorithm

The first step of the existing algorithm was to apply a band-pass filter (250-500 Hz; finite impulse response filter, fstop1 = 240 Hz; fpass1 = 250 Hz; fpass2 = 500 Hz; fstop2 = 510 Hz; stopband attenuation = -60 dB) to the EEG recordings. The signals were filtered forward and backward to obtain zero-phase distortion. The filtered signals were then rectified so as to obtain the amplitude of each oscillatory cycle, which was measured by identifying each "peak" (local maximum) in the rectified data (All negative values in the band-pass filtered data were flipped over and their absolute values were adapted). The histogram of amplitudes in channels where HFOs were not dominant looked very similar to a gamma distribution. However, the presence HFOs, which had relatively high amplitudes, would cause an observable long tail at the end of the distribution, superimposed on the background activity.

Events in which a number of consecutive peaks exceeded a threshold were identified as HFOs. Instead of determining the threshold through visual assessment of characteristics of the signal, like approximate amplitude, we implemented an iterative process to evaluate the amplitude distribution of the signal. In the iterative process, only one parameter indicating the tolerance for false positives was used.

The iterative process was as follows: We modeled the distribution of local maxima in the rectified filtered data with a gamma distribution $f(x)$, whose probability density function can be estimated as:

$$f(x;k,\theta) = \frac{x^{k-1}e^{-\frac{x}{\theta}}}{\theta^k \Gamma(k)} \quad for\ x > 0\ and\ k,\theta > 0.$$

where k and θ are the shape and scale parameters of the gamma probability distribution, respectively and $\Gamma(k)$ is the gamma function evaluated at k. The height of all peaks was used in the first step of the iterative process and k, θ were estimated. These two parameters were then used to construct the probability density distribution *f(x)* to represent the amplitude of background activity. After this, a cutoff of $F(x) = 1 - \alpha$ was defined, where *F(x)* was the cumulative distribution function of *f(x)*. All peaks with amplitude above the cutoff were excluded from the distribution and parameters in the gamma distribution were recalculated for the next iteration. Alpha (α) represented the tolerance for false positive detections and it was directly related to the number of peaks removed in each iteration. For example, if $\alpha = 0.001$, it means the peaks falling in the top 0.1% of the estimated gamma distribution will be removed during each iteration. When $\alpha = 0.1$, peaks falling in the top 10% will be removed. This iterative process continued with k and θ being recalculated until no more peaks were removed. It can be seen that with α increasing, the total number of peaks picked out will increase. In this study, a total of 15 iterations (big enough to ensure no more peaks will be removed) were used to ensure that the estimate of the background distribution had converged (**Figure 2.2**). After the final iteration, we defined the threshold based on the cutoff value of that iteration, as illustrated in **Figure 2.3**. Finally, peaks with amplitudes higher than the threshold were marked and those having a sufficient pre-defined number of consecutive peaks above the threshold were defined as HFOs. All candidate HFOs from the initial detection process were then saved for further processing and analysis. Two detections in one channel separated by less than 10ms were combined into one detection.

We found that, when a single threshold was used for the entire 12-min recording, the performance of the detector suffered. For example, if the mean amplitude of certain parts of

the signal was much higher than the rest, more peaks were extracted from that part (E.g., more peaks would be extracted from a portion of signals with an average amplitude of 40 μV if the average amplitude of the entire channel is 20 μV). In this case, use of only one single threshold led to a significant increase of false detections. Therefore, we made a modification to the existing algorithm based on the characteristics of the EEG signals. Instead of using one common threshold, we divided the signals into 12 parts and calculated a new threshold for each 1-min segment. In this case, setting different thresholds for different parts of the signal helped minimize false detections. Other window sizes, *e.g.* 30 seconds, could be used to make the detection process more precise, but time consumption would be a trade-off.

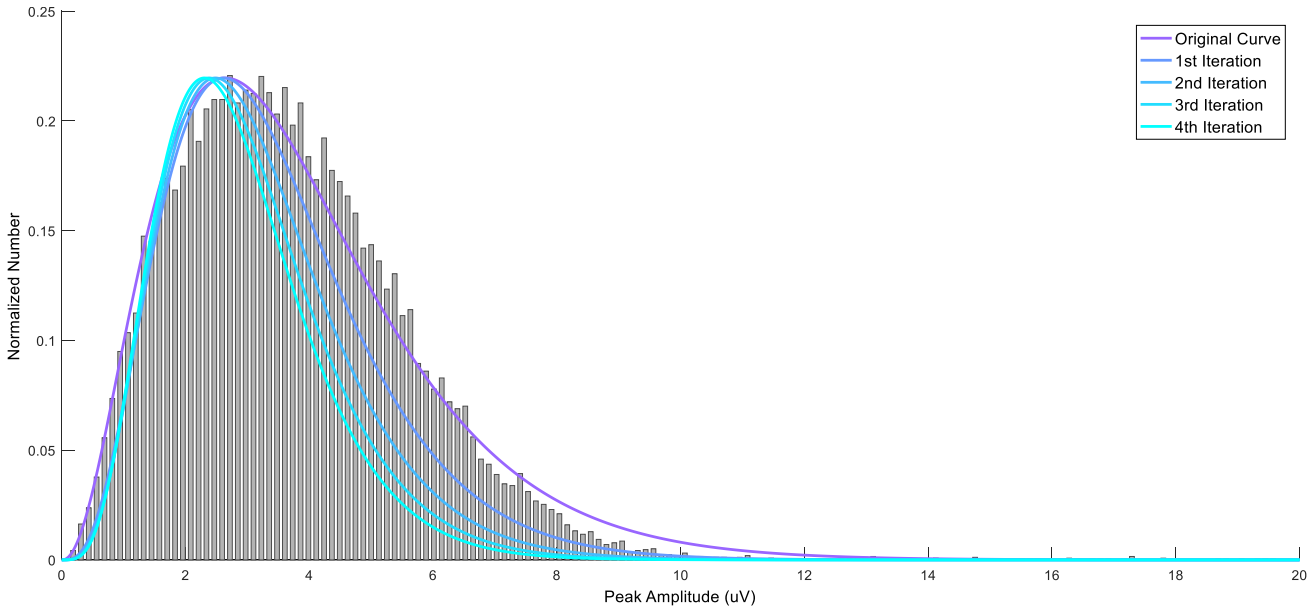

Figure 2.2. Iterative procedure for threshold optimization. The peak amplitude distribution of one channel for both HFO events and background signals are shown using grey bars. The lines represent the estimated distribution curves before iteration and over four iterations.

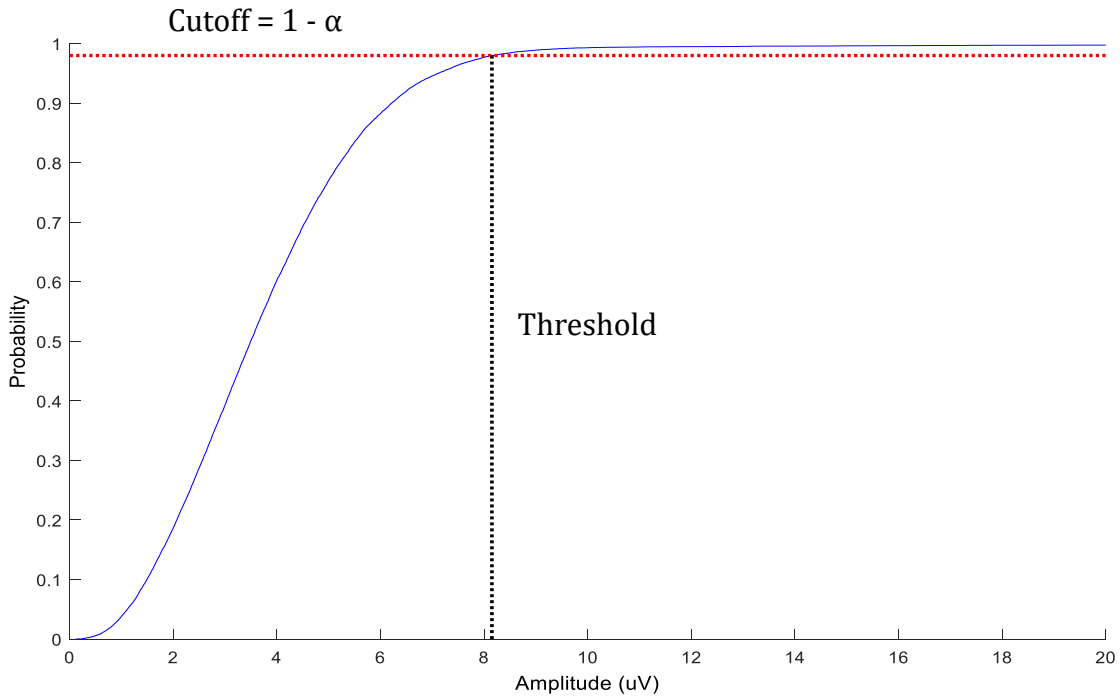

Figure 2.3. The determination of threshold. Threshold is determined using cutoff value 1 – α, which is based on the cumulative distribution function (blue line) of the peak amplitude.

2.3 Post- processing and removal of false detections

In HFO visual annotations, an event is typically assigned to one specific electrode, *e.g.* F7. Therefore, in a candidate HFO pool where the bipolar montage was used for referencing, post-processing of the candidate events was required to combine detections in related channels to one event at one specific electrode.

An example of how two detections with overlap were combined into one event is shown in **Figure 2.4**. A segment of band-pass filtered signal from two channels is displayed,

while two detections in channels C4-P4 and P4-O2 are marked in red. The signal between the two blue dashed lines is the area of overlap between two channels, and the two solid red lines mark the beginning and end of the entire event. During post-processing, if this type of paired detection appeared, we calculated the length of the overlapped segment. If the length of the overlapped segment was higher than 30% of the length of the entire event, the detections in two channels both related to electrode P4 would be combined as one event. This event would be defined as a candidate HFO in channel P4. In the case where the length of the overlapped segment is lower than 30% of the length of the entire event, both detections are considered as separate events. In the example in Figure 2.4, both detections would be combined into one candidate HFO event in channel P4. (**Figure 2.4**)

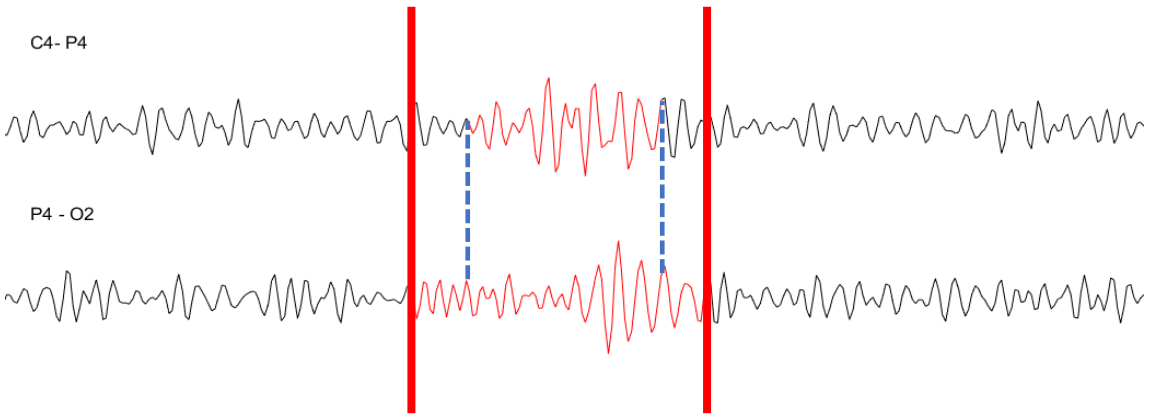

Figure 2.4. Combination of two detections into one event. Signal between two blue dashed lines is the overlapped area between two channels. Two red solid lines mark the beginning and end of the event after combining two detections together.

Dealing with false detections is challenging for HFO automatic detectors, especially for those using EEG data. The analysis of HFOs is commonly focused on the fast ripple band (250 ~ 500Hz in this study). Many different kinds of artifact and noise-like muscle artifacts,

sharp transients, eye movements, epileptic spikes and electrode noise artifacts can be associated with high spectral power in the fast ripple band. This can cause events that look like real HFO events in the fast ripple band and to be falsely detected by the algorithm. Therefore, these spurious events should be removed from the candidate HFO pool after the initial detection.

Three false positive rejection methods were applied to the initial detection pool. (1) First, raw signal was evaluated. One of the most typical characteristics of noise is its chaotic oscillation around the zero-line (Liu et al. 2016). Therefore, we proposed a simple method to remove this kind of noise. If the raw signal of the candidate HFO crossed the zero-line more than five times during the event interval, it was treated as noise and was rejected from the candidate pool. (2) The next step was to examine the band-pass filtered signal in successive 1-second windows. If the maximum amplitude in a 1-sec window was higher than 60 μV, all candidate HFOs in that 1-sec period were removed (**Figure 2.5**). The purpose of doing this was to imitate the detection process by human reviewers: if irregular waveforms with extremely high amplitude appeared in a 1-sec window, it would usually be regarded as artifact caused by body movement or other noise. In that case, no HFO event would be marked in that window. (3) The third false detection removal method was designed specifically for recordings using a bipolar montage, due to the fact that each channel is related to two different electrodes. HFOs are typically seen in more than one channel and will have the highest amplitude in the channel pair closest to the source. Therefore, we were looking for events that had a "field," evidenced by correlated activity across channels. We used zero-lag cross correlation in this method to evaluate the similarity between two time

series. Cross correlation is also known as a sliding dot product or sliding inner-product, and it can be defined as:

$$(f * g)(\tau) = \int_{-\infty}^{\infty} f^*(t)g(t+\tau)dt$$

where f^* is the complex conjugate of f and τ is the displacement, or lag.

A number of tests were done to determine the threshold value which separated "high correlation" and "low correlation", which was determined to be 0.7 in this study. For example, if there was a candidate HFO in channel F7-T3, the zero-lag cross correlation between channel F7-T3 and Fp1-F7, channel F7-T3 and T3-T5 was calculated. The candidate HFO in channel F7-T3 was regarded as a false detection and removed if both cross-correlation values were lower than 0.7 (**Figure 2.6**). In other words, only when the "similarity level" between those two pairs of signals was high, was that detection reserved for further analysis. (**Figure 2.7**)

In some datasets, one of the most prevalent artifacts is a DC shift, a kind of wide-band fast activity. Clinicians could easily identify this activity as artifact in the raw data, but when the raw signal is band-pass filtered for HFO processing, it can appear identical to an HFO. We proposed a method in our artifact rejection procedure to remove these shifts by looking at the signal band-pass filtered in 850~990 Hz (Gliske et al. 2016). Normal neural activities and HFO events usually have significantly attenuated amplitude in this frequency band compared to the fast ripple band. However, due to their spectral characteristics, DC shifts maintain relatively high amplitudes in this frequency band, causing them to stand out from the background activity. The published paper made use of the line-length of a 0.1 second window of 850~990Hz band-pass filtered data, however we hypothesized a thresholding method

could be helpful in the removal a DC shift. In this method, we defined a detected event as a DC shift based on the criteria below:

$$Max\_Amplitude[E(i)] - Min\_Amplitude[E(i)] \geq Threshold(i)$$

where E stands for each automatically detected event and i is the label for that event.

An example of a DC shift is shown below in **Figure 2.8.**

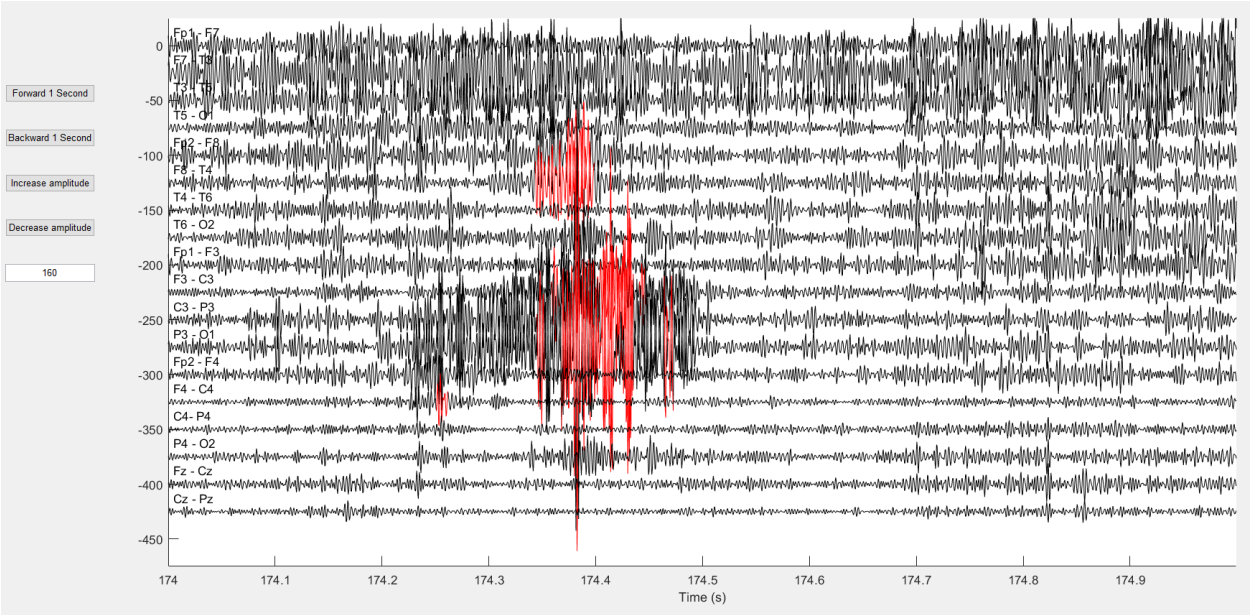

Figure 2.5. Example of noise appearing in detection results. Signal marked in red has a maximum amplitude higher than 60 μV and will be treated as noise, thus all detections in this window will be moved.

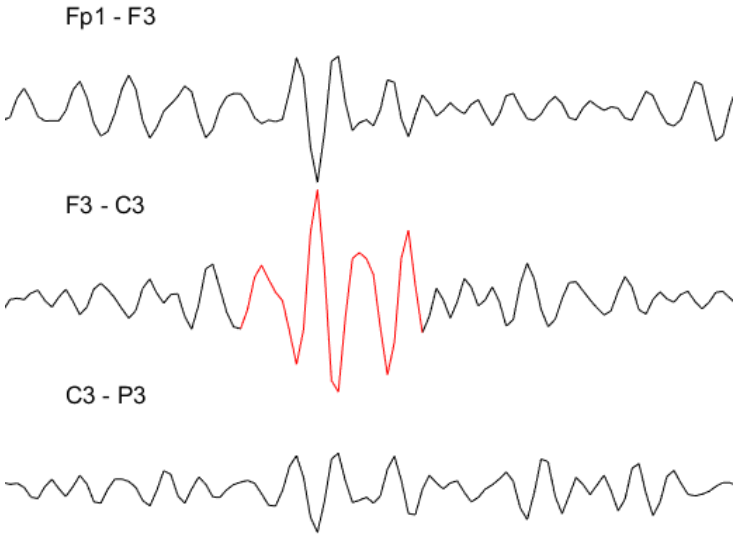

Figure 2.6. Example of an automatic detection which has low correlation with related channels.

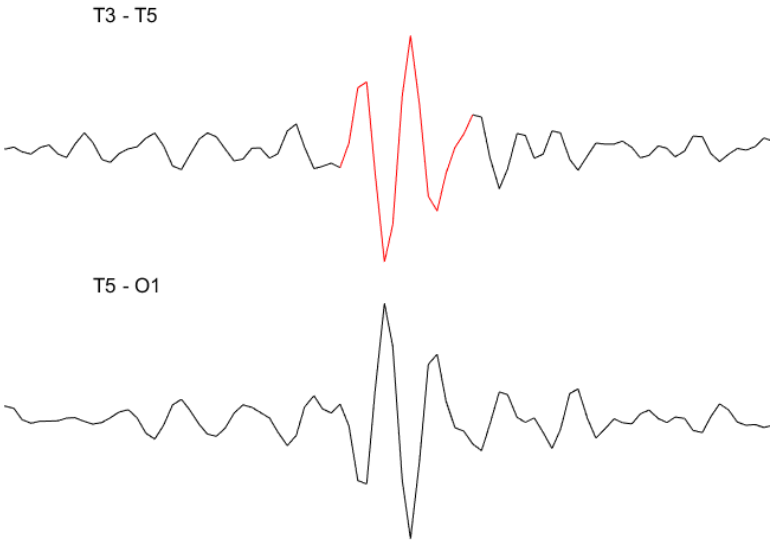

Figure 2.7. Example of an automatic detection which has high correlation between two related channels.

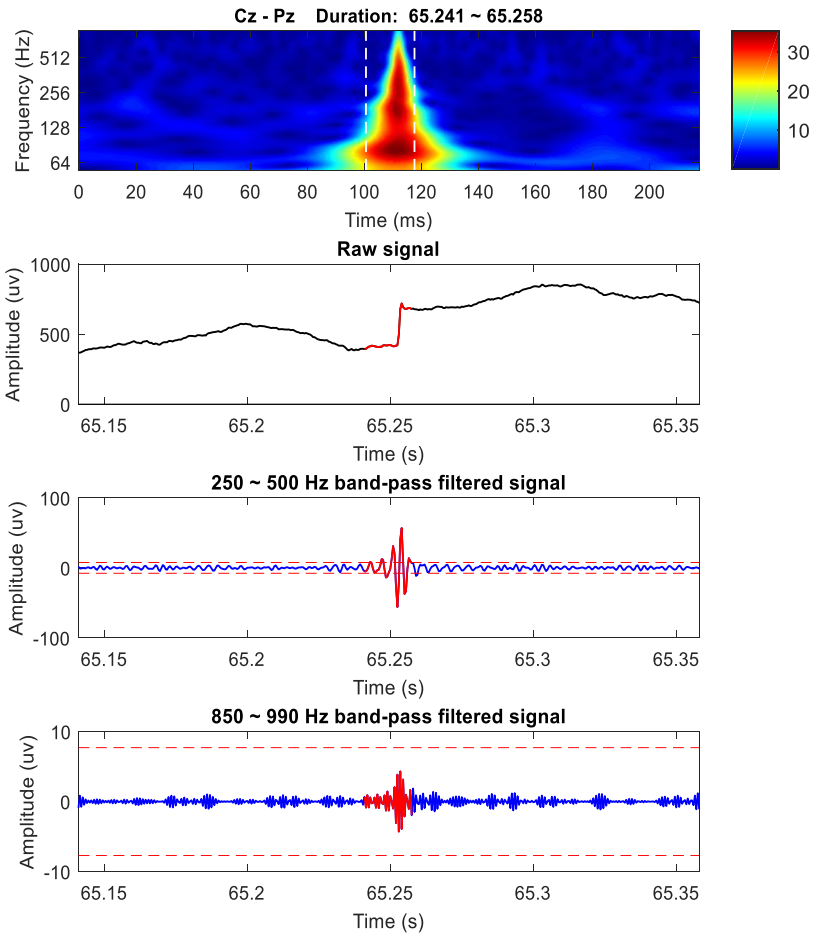

Figure 2.8. Example of DC shift. It can be easily rejected by examining the time-frequency map and raw signal. In the former, the high energy is spread widely throughout the whole frequency band (top panel), and in the second panel a sharp transient is observed in the raw data.

2.4 Visualization of HFOs

We built a user-friendly graphical user interface in MATLAB to display all candidate HFOs, as shown in **Figure 2.9**. The purpose of designing this interface was to build an environment similar to the Persyst software in which visually marked HFOs were annotated. We built a Persyst-like environment for ease of usage in a research environment, making it easier to adjust features of the display and providing better visualization of HFOs in the interface.

In this environment, 1-second of 250-500 Hz band-pass filtered EEG signal referenced with a bipolar montage was displayed in one window with channel labels on the left. There are four buttons on the left of the panel indicating “Forward 1 Second”, “Backward 1 Second”, “Increase amplitude”, “Decrease amplitude” respectively and they help the user change the time range displayed and the desired amplitude resolution. Below these four buttons there is a box where the user can input any value of time within the range of the entire EEG recording and jump to a desired time point quickly. The background signals are shown in black and all candidate HFOs detected using our algorithm are shown in red. (**Figure 2.9.**)

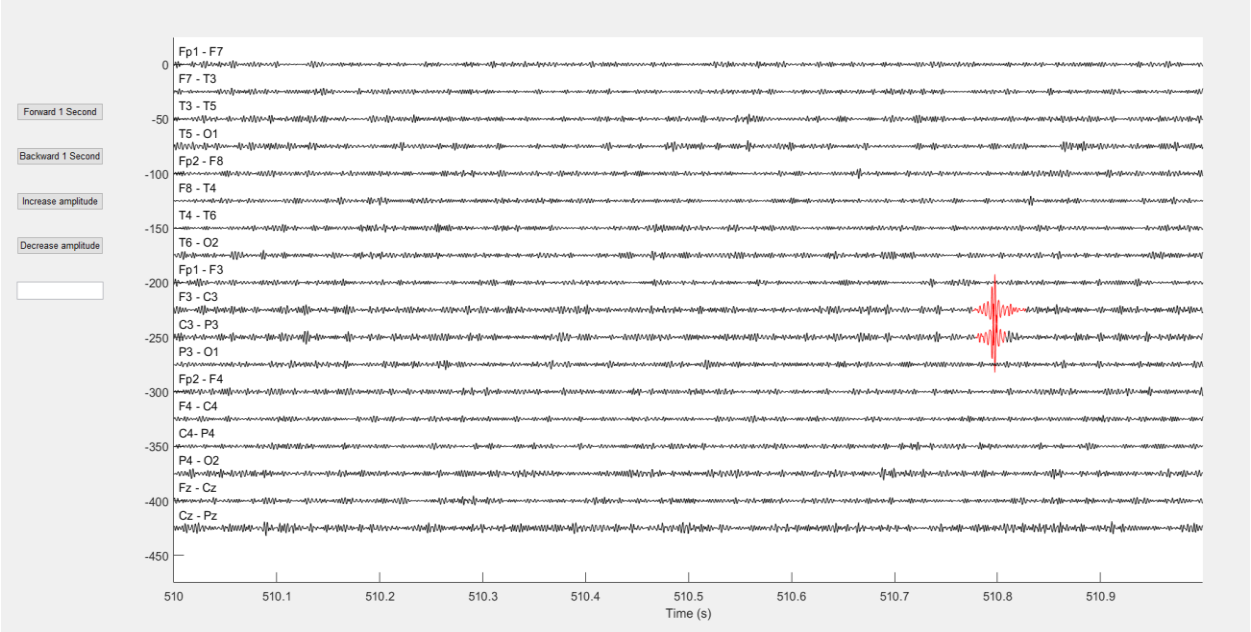

Figure 2.9. Persyst-like interface. Signals in red mark two automatically detected events in channels F3-C3 and C3-P3.

For the purpose of designing suitable artifact rejection methods for candidate events, we performed a visual validation of the detected events. After the initial extraction of automatic detections, each event was reviewed separately by looking at its raw signal, filtered signal (fast-ripple band) and time-frequency map. An Analytic Morse Wavelet analysis was employed to generate the time-frequency map. It was reported that the Morse wavelet was more appropriate to describe the temporal characteristics of the frequency content of HFOs compared to other commonly used time–frequency decomposition methods (Amiri et al. 2016). In the Fourier domain, the equation for Morse wavelet is denoted as:

$$\psi_{\beta,\gamma}(\omega) = U(\omega) a_{\beta,\gamma} \omega^{\beta} e^{-\omega^{\gamma}}$$

where γ characterizes the symmetry of the Morse wavelet, β can be viewed as a decay or compactness parameter and $a_{\beta,\gamma}$ is a normalizing constant.

An example of an HFO with its raw unfiltered signal, band-pass filtered signal and time-frequency map is shown in **Figure 2.10.**

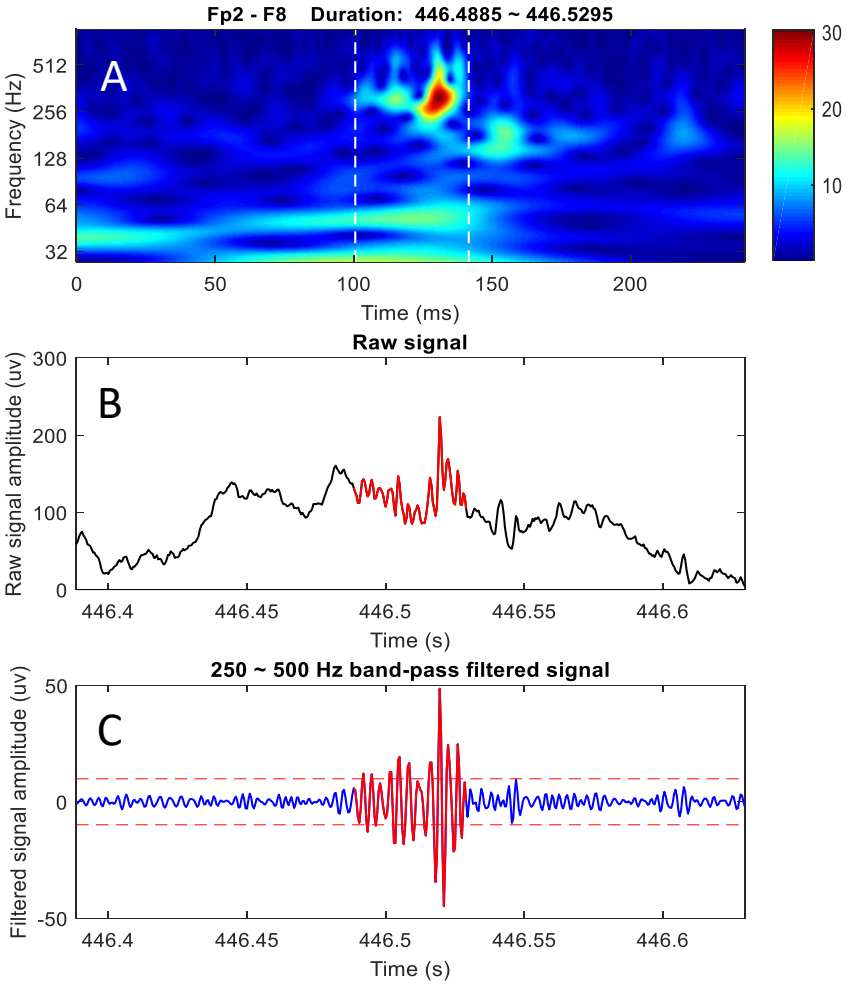

Figure 2.10. Example of an HFO event in fast ripple band. (A) Morse wavelet time-frequency presentation of the HFO event, where the white vertical dashed lines represent the duration of the event and different colors in the map stand for energy (red for high energy, blue for low energy). (B) Raw signal of the event with 0.1s before and after. The red trace represents an automatically detected event. (C) 250 ~ 500 Hz band-pass filtered signal of the event. Red horizontal dashed lines are the threshold.

2.5 Optimization of parameters and evaluation of detector performance

Two parameters needed to be optimized in this algorithm: α and the ratio of NPEAKTH/NCYCLES. α is the parameter that determines the percentage of peaks selected in the iterative process and is related to the tolerance for false positive events. NCYCLES means the minimum number of peaks in each detected event, while NPEAKTH stands for the minimum number of peaks above the threshold in each detected event. We tested the detector using different parameter combinations and evaluated the detector performance in order to find the optimum parameter combination for each patient. The performance of the automatic detector was evaluated via an ROC curve, which was plotted using TPR (True positive rate) and FDR (False detection rate). To calculate TPR and FDR, true positives (TP) were defined as detected events that matched the visually marked HFOs. If the length of overlap between detected events and one specific visual marking was larger than 30% of the visual marking, that event was defined as a true positive. False positives (FP) were automatically detected events that were not visually annotated. False negatives (FN) were HFO events which were visually marked but not automatically detected. Then sensitivity (TPR) was defined as TP/(TP+FN), and FDR was defined as FP/(TP+FP). The optimum value of α was chosen by identifying the best balance between sensitivity and FDR, the point on the ROC curve that was closest to the upper left corner of the plot. The performance at this optimum value illustrates the best possible performance of the detector.

After we optimized the parameters and evaluated the detector performance, the candidate HFOs using the best parameter combination were obtained. The whole procedure is displayed in the flowchart in **Figure 2.11.**

2.6 Robustness across patients within different groups

In practice, it would be unrealistic to complete visual detection and perform the optimization of threshold on all channels due to large number of channels. Therefore, to optimize the parameter α, we cannot assume that prior knowledge of "true" events is available. Here we tested the robustness of the detector across patients. This is a stringent test of performance because the peak amplitude distributions and detected event distributions could vary significantly among different patients due to the different background characteristics. For this test, we divided all datasets into two groups based on their signal-to-noise ratio (SNR), where Group 1 has a high SNR and Group 2 has a low SNR. We did this because we anticipated that the two groups would require different detection parameters. The most important feature of datasets with high SNR (Group 1) was that most detections were concentrated in less than five channels and visually marked HFOs typically stood out from the background. In datasets with low SNR (Group 2), the distribution of detections was relatively uniform across all eighteen channels and visually marked HFOs didn't stand out as obviously as those in Group 1. Therefore, we grouped the detection results in Group 1 and Group 2 separately, analyzed the detector performance in each group and found the optimum parameter combination that gave the best results in each group. A similar strategy was used for an existing automatic HFO detector applied to depth EEG data, where channels with nearly continuous high frequency activity or less than one visually identified HFO or baseline were assigned to a separate sub-group (Zelmann et al. 2010).

2.7 Leave-one-out cross-validation

We applied two leave-one-out cross-validation tests to all datasets in order to evaluate the detector performance.

The first test was done within each group of datasets. In Group 1 (Patient I, II, III), one dataset was selected for testing and the other two datasets were used for training, while in Group 2 (Patient IV, V, VI, VII) one dataset was selected for testing and the other three datasets were used for training. In the training procedure, the detection results of the training datasets were grouped together, ROC curves were plotted and the point on the ROC curves having the best balance between TPR and FDR was chosen as the optimum point. Then the optimum parameter combination was applied to the test dataset. The test result was obtained by averaging the results from each individual test.

Different from the first test, the second cross-validation test was completed across all seven datasets, where six datasets were used as training data to test on the remaining dataset. The procedure was repeated seven times as each dataset was used once for testing. This tests the robustness of the algorithm independent from the Group 1 and Group 2 designations.

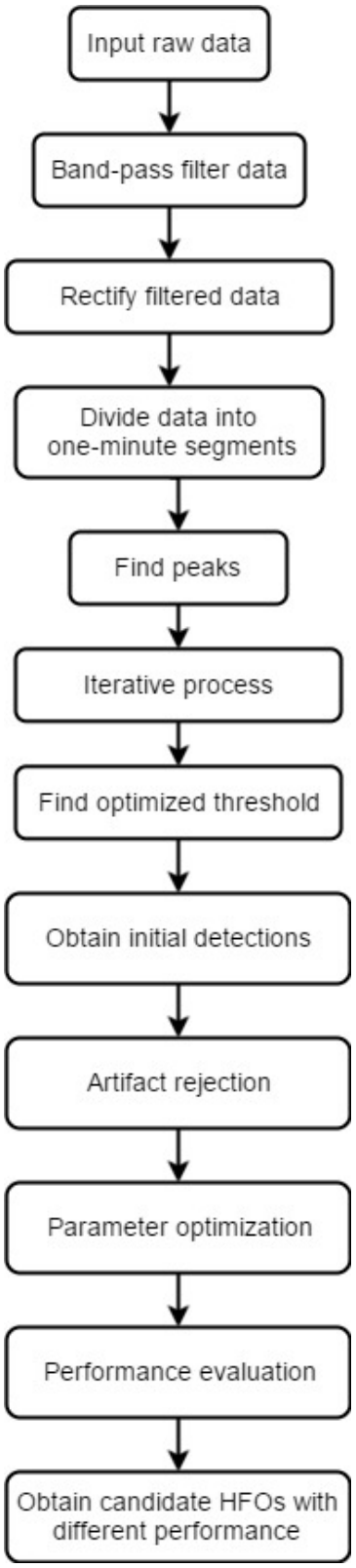

Figure 2.11. Flowchart of the detection process.

Chapter 3 Results

3.1 Detector performance

We evaluated the performance of our detector by calculating ROC curves for each patient. In each plot, there are nine curves representing nine "NEAKTH/NCYCLES" combinations, namely 4/5, 4/6, 4/7, 5/6, 5/7, 5/8, 6/7, 6/8, 6/9. In each curve, a series of alpha values ranging from 0.0001 to 0.035 was used to evaluate the detector performance. The point on each curve closest to the upper left-hand corner was regarded as the point where there was the best balance between TPR and FDR, and the parameter combination at that point was defined as optimum parameter set. **Figure 3.1.** shows the ROC plots illustrating the detector performance in all seven patients. Since these plots depict the relationship between TPR and FDR, the performance curves could lie below the chance line (TPR = FDR), instead of the classical ROC curve (TPR vs FPR), which normally lie above the chance line (TPR = FDR).

Using the points with the best balance between TPR and FDR in seven patients, our detector had an average sensitivity of 86.3% with FDR of 11.3%. When better sensitivity was desired and the highest acceptable FDR was 50%, we obtained a TPR of 91.2% and FDR of 31.7%. The highest TPR we obtained regardless of the number of false positives was 95.3%. All results above were obtained when we used different parameters for each patient. If we used the same parameters within all seven patients, we obtained a TPR of 85.0% and FDR of 38.3%. In this case, the optimum parameter combination within all patients was $\alpha = 0.005$, NEAKTH/NCYCLES = 5/7.

We noticed a significant difference between datasets in Group 1 and Group 2. Much better performance was observed in Group 1, where most HFOs stood out obviously and occurred regularly in less than five channels **(Figure 3.2)**. However, in the other four datasets, worse performance occurred because a large number of HFOs didn't stand out from the background activity (**Figure 3.3**). Achieving a high sensitivity would incur a high false detection rate. If we tested the detector performance using the same parameters within each group, the detector had a sensitivity of 84.6% and FDR of 36.8%.

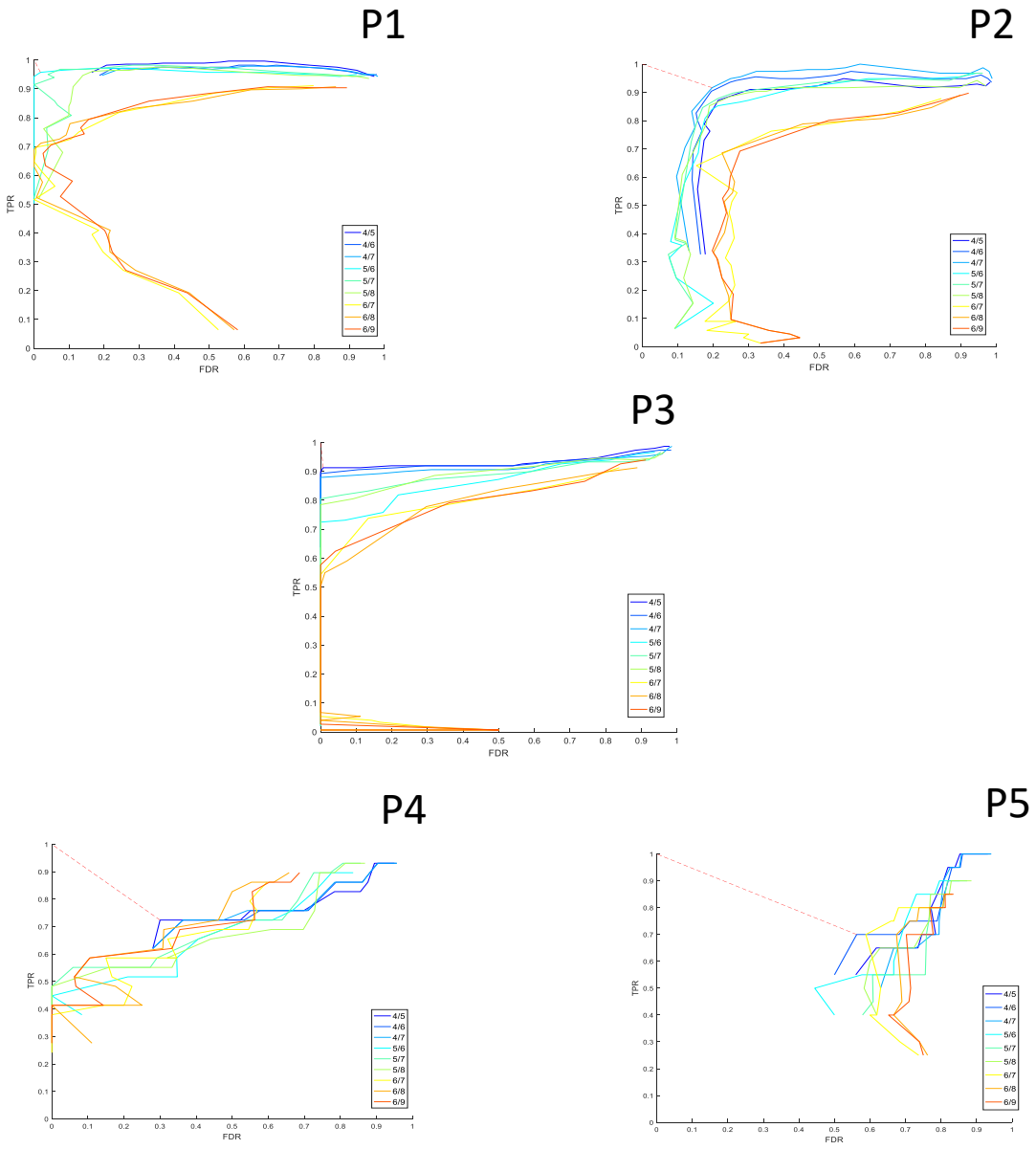

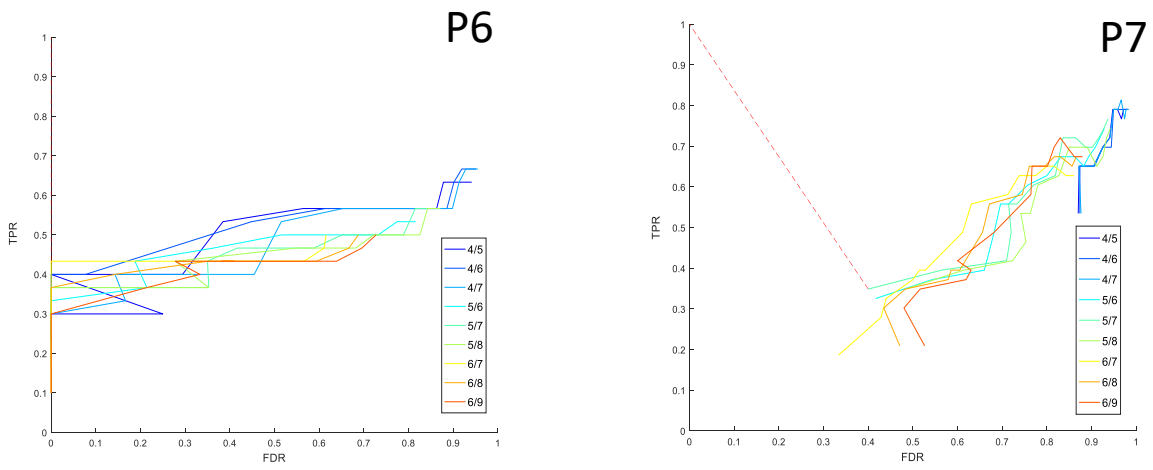

Figure 3.1. FDR-TPR plot for seven patients. Each curve contains a variety of α values. The red dashed line in each plot connects the upper left corner to the point with the best balance between TPR and FDR.

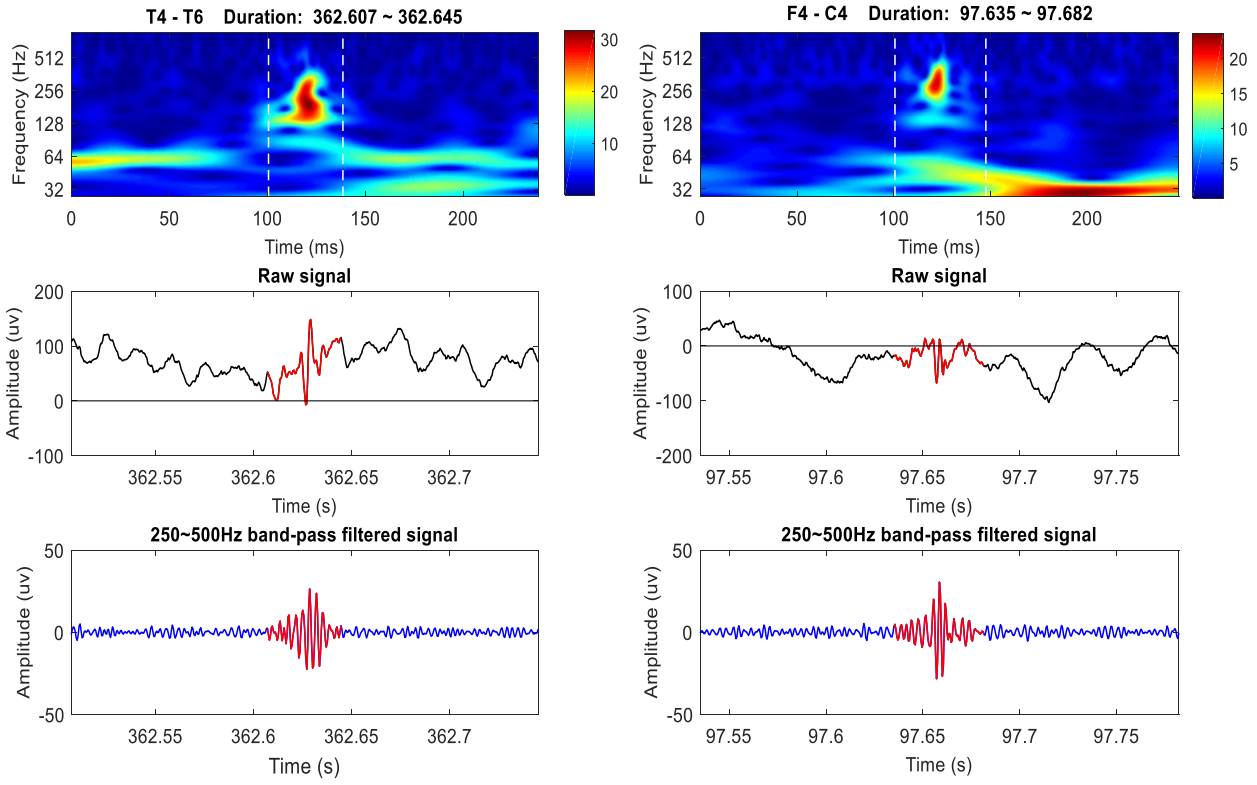

Figure 3.2. Example of fast ripple events which stand out from background activities.

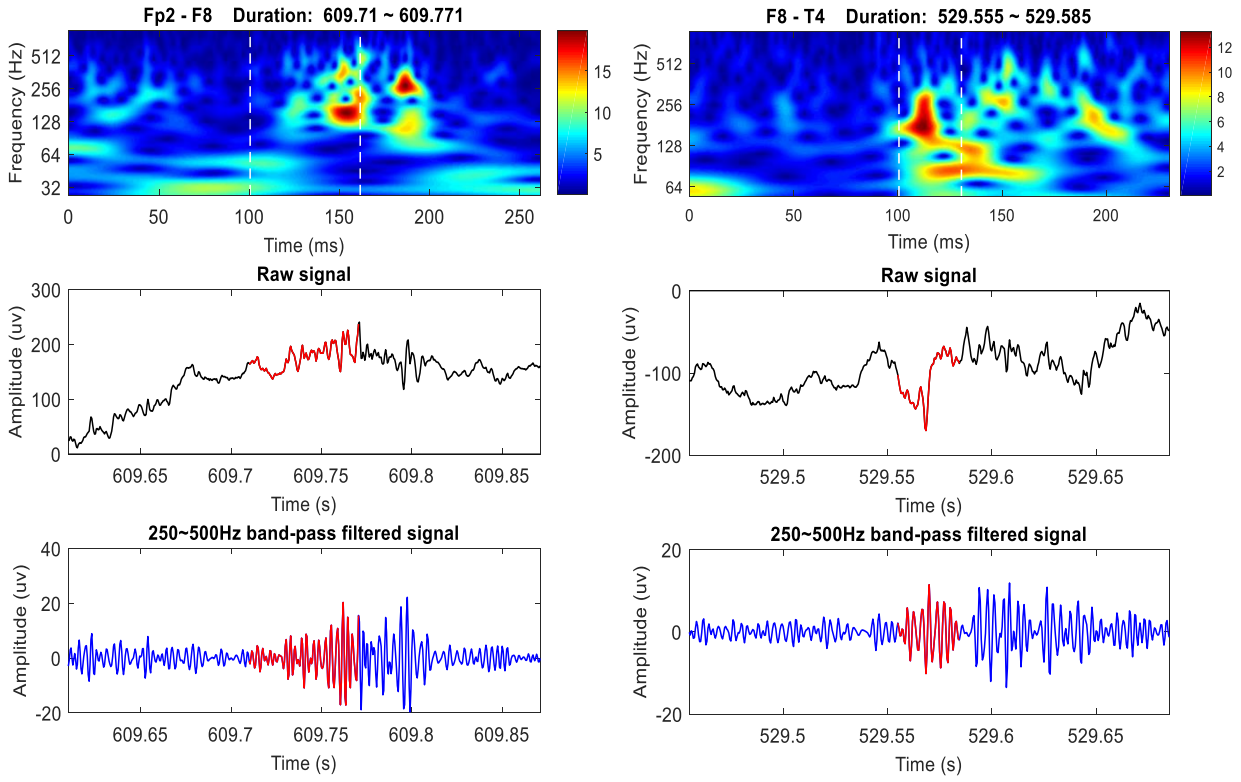

Figure 3.3. Example of fast ripple events not standing out from background activities.

3.2 Robustness of detector across patients within each group

Figure 3.4. and **Figure 3.5** show the distributions of detections in the seven patients studied in this project. Based on the ROC curve and detection distribution of each patient, we found that for Patients I, II and III, the optimum α value ranged from 0.0007 to 0.005, while 4 out of 5, 4 out of 6 and 4 out 7 consecutive peaks all provided satisfactory results (TPR>80%, FDR<50%).

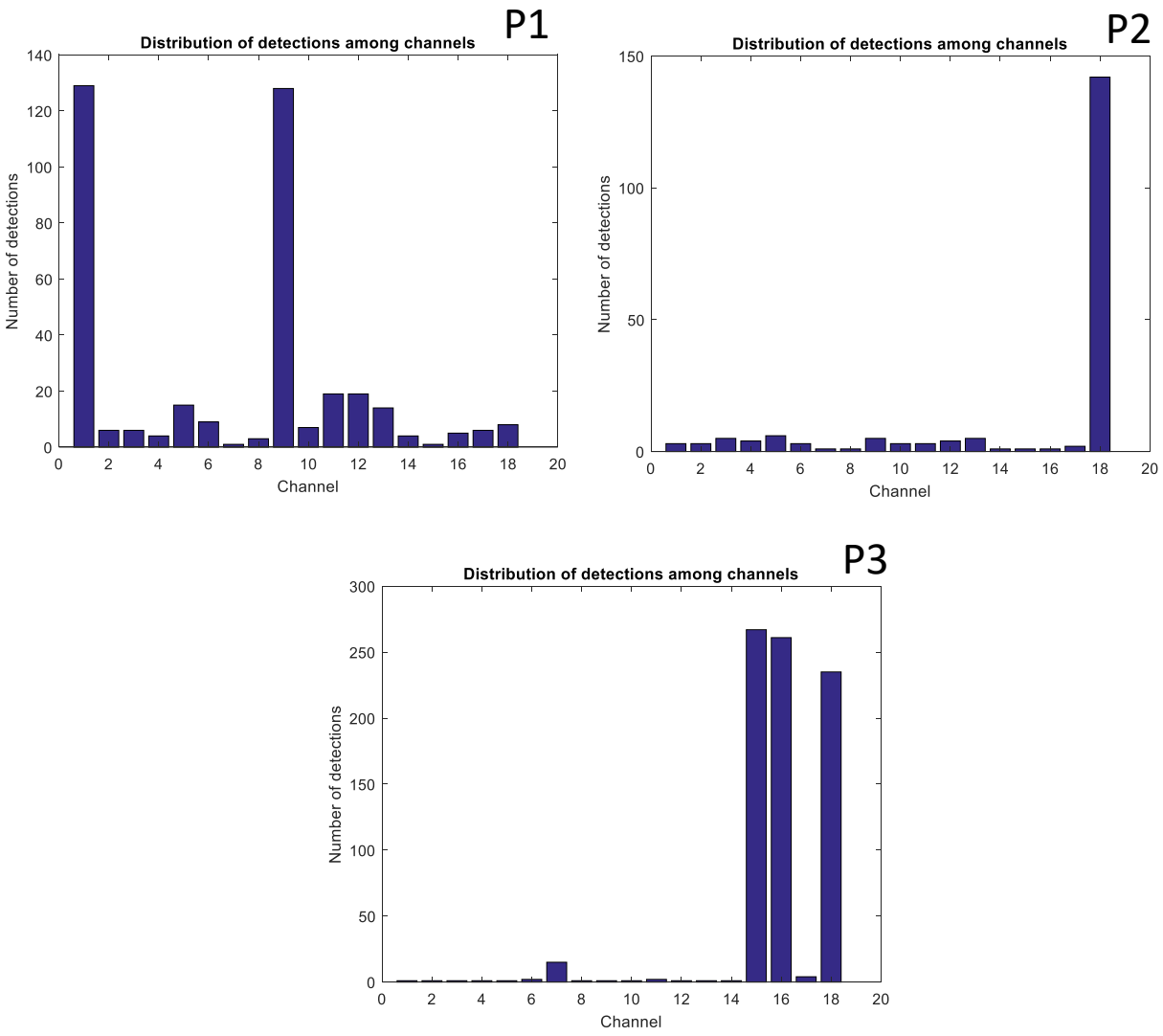

Figure 3.4. Detection distribution of datasets with high SNR. (Group 1)

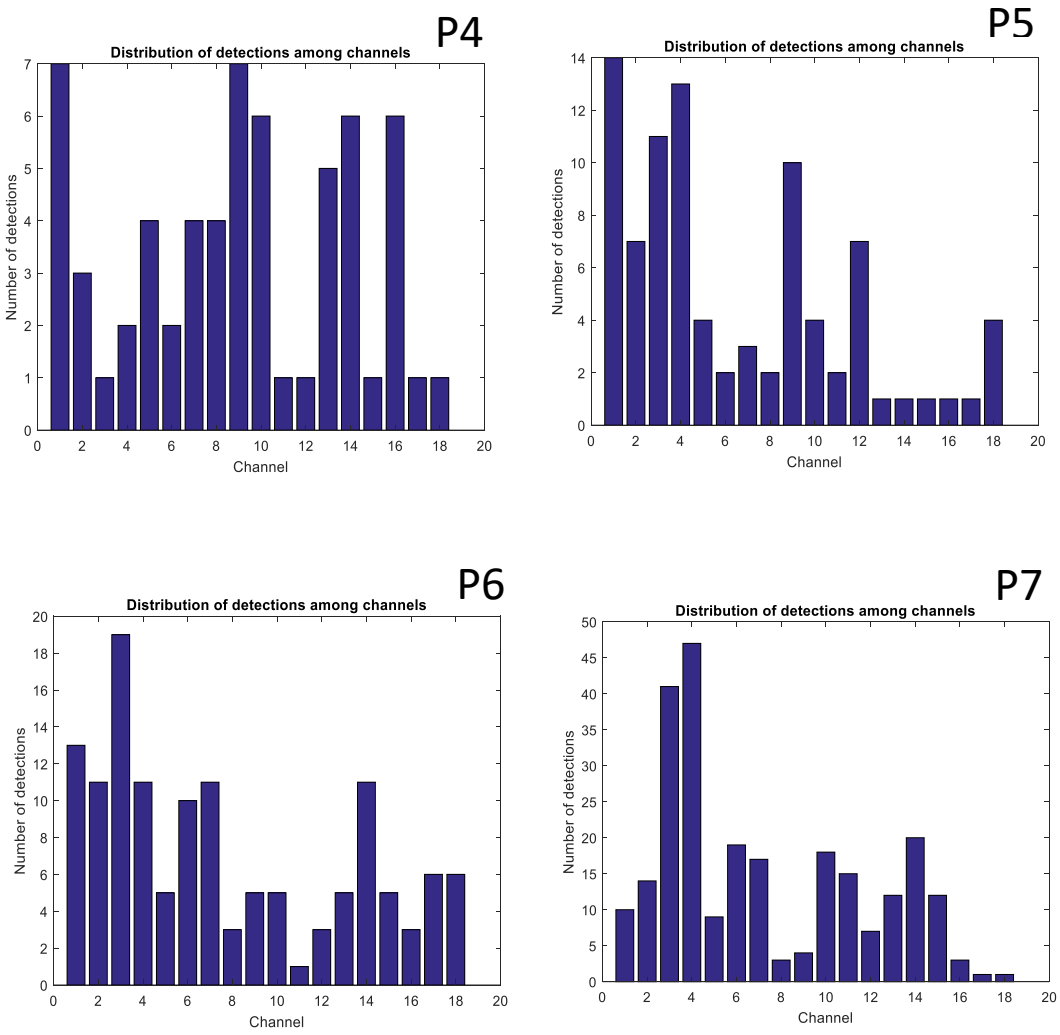

Figure 3.5. Detection distribution of datasets with low SNR. (Group 2)

To determine the parameter combination that gave the best results, we grouped all events within the first three patients together, summarized the detector performance and plotted an ROC curve as shown in **Figure 3.6**. 5 out of 7 consecutive peaks with $\alpha = 0.005$ was set as the detection criterion and it gave a sensitivity of 88.4%, while FDR equaled 8.6%. If higher sensitivity was desired with maximum FDR lower than 50%, the detector gave a TPR of 95.7% and FDR of 49.3%. In that case, α was 0.006 and 4 out of 7 consecutive peaks

were defined as criterion. When lower false detections was desired with minimum sensitivity of 85%, we obtained a TPR of 88.4% and FDR of 8.6%.

For Patients IV, V, VI and VII, the optimum α value ranged from 0.0001 to 0.002. 5 out of 7 and 6 out of 7 consecutive peaks gave relatively good results (points closest to the upper-left corner), but incurred many more false detections when compared to the first three patients. **Figure 3.7** gives a specific illustration of the result. When α = 0.002 and 6 out of 7 consecutive peaks are used as the detection criterion, the best balance between TPR and FDR results in a TPR of 50.8% and FDR of 47.5%.

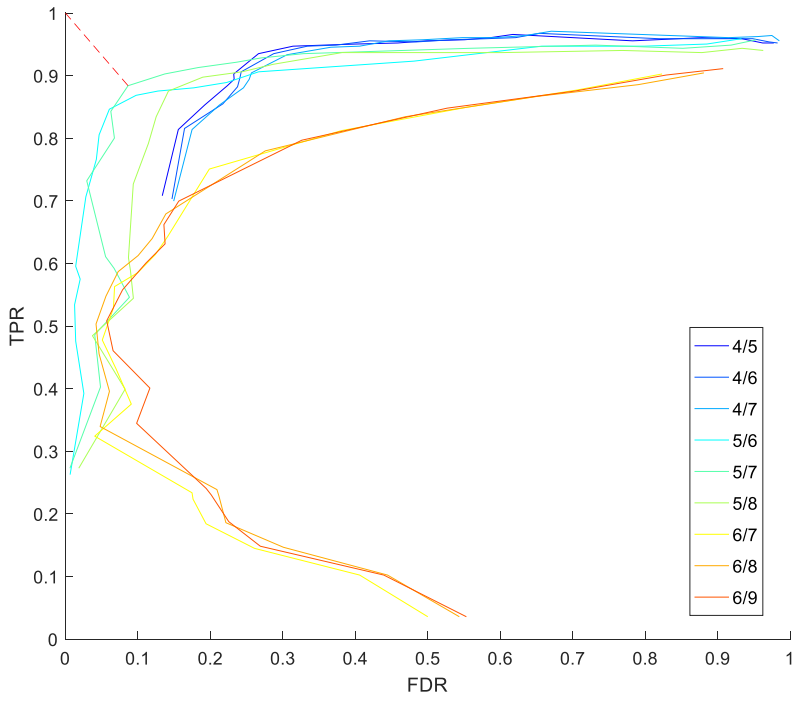

Figure 3.6. FDR-TPR plot averaged across Patients I, II and III. Each curve contains a variety of α values. The red dashed line in each plot connects the upper left corner to the point with the best balance between TPR and FDR.

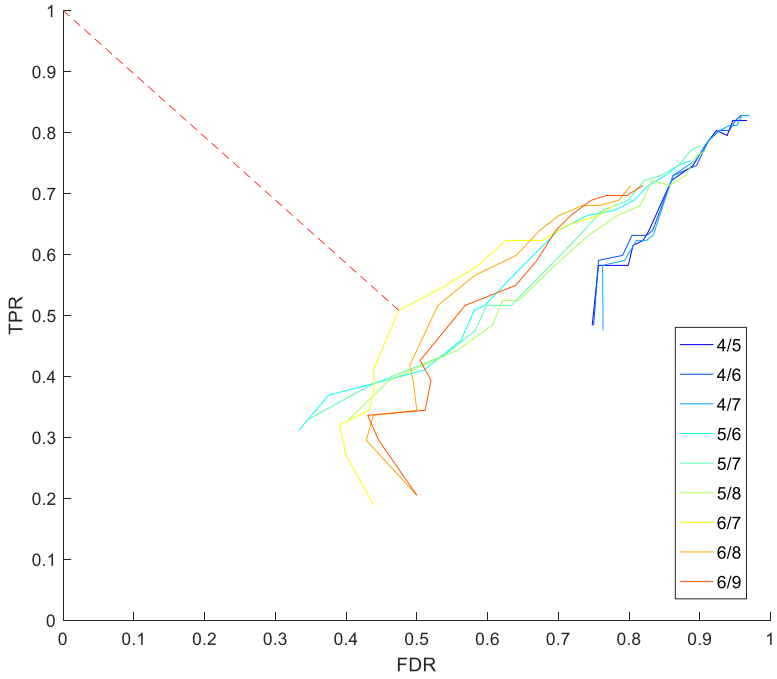

Figure 3.7. FDR-TPR plot averaged across Patients IV, V, VI and VII. Each curve contains a variety of α values. The red dashed line in each plot connects the upper left corner to the point with the best balance between TPR and FDR.

3.3 Leave-one-out cross-validation

When we did the cross-validation test across all seven patients, the optimum alpha value ranged from 0.002 to 0.004 and the best values of NPEAKTH/NCYCLES were 5/6 and 5/7. The detector obtained an average TPR of 71.5% and FDR of 36.2%.

When the test was done within the two different groups separately, we obtained a TPR of 86.5%, FDR of 29.7% in Group 1 and a TPR of 50.8%, FDR of 50% in Group 2. The optimum alpha values in Group 1 were 0.002 and 0.005, while optimum NPEAKTH/NCYCLES value were 4/6, 5/6 and 5/7. In Group 2, the optimum NPEAKTH/NCYCLES value was 6/7 while the best α values were 0.002 and 0.003.

The statistical results for our detector across all seven patients are shown in **Table 3.1**.

Table 3.1. Detection statistics of the detector

	Sensitivity (%)		**FDR (%)**	
	Mean ± SD	**Min, Max**	**Mean ± SD**	**Min, Max**
Average across 7 patients (Optimum parameters used, different α for each patient)	86.3 ± 24.2	34.9, 95.7	11.3 ± 22.0	0, 56.2
Average across 7 patients (Highest TPR with FDR<50%, different α for each patient)	91.2 ± 16.6	53.3, 98.2	31.7 ± 28.3	7.3, 76.1
Average across 7 patients (Same α for each group)	84.6 ± 15.5	46.7, 96.8	36.8 ± 35.0	0, 86.4
Average across 7 patients (Same α for all patients)	85.0 ± 15.3	46.7, 96.8	38.3 ± 36.3	0, 86.4
Leave-one-out Cross-validation (Within all 7 patients)	71.5 ± 18.4	43.3, 95.0	36.2 ± 36.0	0, 86.3
Leave-one-out Cross-validation (Within Group 1)	86.5 ± 14.9	67.8, 97.5	29.7 ± 20.4	0, 40.6
Leave-one-out Cross-validation (Within Group 2)	50.8 ± 15.5	33.3, 70.0	50.0 ± 28.4	0, 61.1

Chapter 4 Discussion and conclusion

Here we proposed a simple automatic detection algorithm for fast ripple events in scalp EEG based on an existing algorithm which we adapted to scalp EEG data. We applied several artifact rejection methods to remove false detections due to the fact that scalp EEG can easily be influenced by artifacts and noise. Also, we built a Persyst-like environment in MATLAB to provide better visualization of detected HFOs and we implemented time-frequency analysis to help optimize detection parameter sets. In this algorithm, two parameters needed to be optimized through an iterative process based on the statistical characteristics of the background activity. Parameter α is directly related to the value of the threshold, thus making the sensitivity and specificity of the detector dependent on the change in α. Another parameter, NPEAKTH/NCYCLES, determines the minimum number of qualified peaks and minimum duration of detected events. The performance of the detector was promising, especially in subjects with clear HFOs that stood out obviously from the background. Therefore, we believe this algorithm could be a suitable technique for the detection of fast ripple HFO events in scalp EEG.

We also implemented several methods for artifact rejection. These methods made the detector more robust, as we saw a significant drop in the number of false detections after applying these techniques. In addition, we examined the detection distribution among channels within each dataset and found that this led to the categorization of patients into two groups. We optimized the parameters within each group independently and found different optimum parameter combinations for them. Using different parameters between the two groups gave us better results than using the same parameters within all datasets.

This could aid in the optimization process for the analysis of new datasets where prior visual markings are not available.

Although this detector is advantageous compared to some published algorithms due to its simplicity in parameter optimization and application, there are still a number of important questions to be addressed. First, the performance of the detector varies dramatically in different datasets due to the differences in signal features, including the amplitude and duration of HFOs and the presence of artifacts. The detector works much better in datasets where the majority of HFOs appear in less than five channels, where they usually had higher amplitude and stood out from the background. However, in datasets where HFO events are widely distributed, the number of false detections increased significantly although high sensitivity can be obtained.

Second, we found that the duration of visually annotated events is typically longer than automatically detected events because reviewers are more likely to include more data before and after HFO events. Therefore, some possibly real events barely passing the minimum duration requirement will be missed by reviewers because they are not long enough. In addition, even though detections in a channel separated by less than 10ms were combined as one detection, it is very challenging for the detector to provide good performance when human reviewers marked events with extremely long duration (*e. g*. >100ms) as shown in **Figure 4.1**. It is vital that these visual assessment criteria are accurate and precise so that better criteria for automatic detection can be set up. Furthermore, events with high frequency components like DC shift, fast transient and epileptic spikes were easily mistaken in visual markings for high frequency oscillations due

to their similarity with HFOs in fast ripple band. However, these artifacts can be easily rejected if their raw signal is compared to the raw signal of HFOs. Therefore, we believe it is necessary to look at the raw signal, fast ripple band and even a higher frequency band of the recording when doing visual annotations so that high accuracy can be guaranteed. Also, a time-frequency map can be used to provide concrete information regarding frequency resolution. In this algorithm, we hypothesized that HFOs are rare events, thus their high amplitude would obviously differentiate them from the background signal. If these events appear frequently in one channel, or in multiple channels in one time window, the method we used to estimate amplitude distribution and optimize the threshold would be inaccurate and cause a drop in detector performance. However, channels with frequent HFO appearances are also challenging for human reviewers to mark, so this problem is not specific to automated detection.

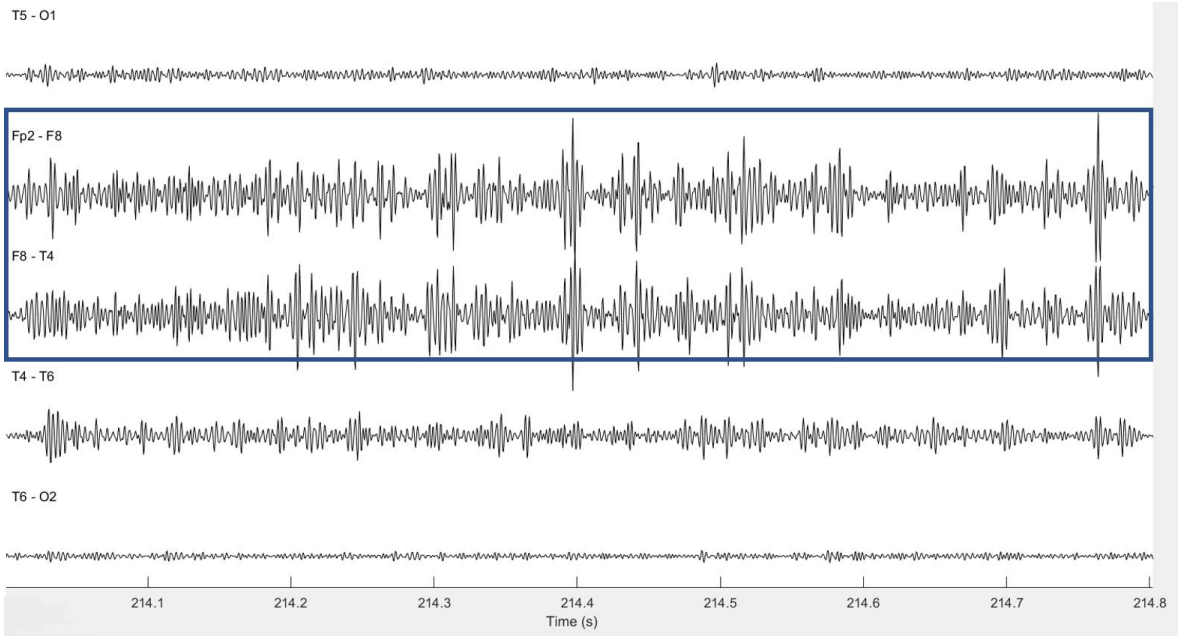

Figure 4.1. Example of a visual annotation with long duration. The filtered signal in the blue rectangle represents one visually marked HFO in channel F8 with a duration of approximately 1 second.

Third, the high number of falsely detected events remains a challenge in the implementation of automated detection. The most common reason for false detections is that the oscillations have just enough peaks exceeding the threshold but don't stand out obviously from the background signal (**Figure 4.2**). Also, reviewers do not tend to mark an event if there are higher amplitude events nearby that are marked. This is directly related to the value of the threshold. For this reason, we modified the detection procedure by dividing the entire recording into multiple 1-minute segments. The value of threshold changed in each 1-minute section, but the alpha value was pre-defined and remained constant in the whole detection procedure. By doing this, the threshold in different time periods of the recording was more accurate, leading to better performance. For example, a large amount of artifact with extremely high amplitude can be avoided if a higher threshold is used in this period compared to the minute after or before. We chose one minute as our window size when segmenting the recording. A smaller window size, *e.g.* 30 seconds can be applied to provide more thresholds for each channel, but high time consumption could be a problem. With our computer system (CPU: Intel I7-6700, 8 GB of RAM with solid state drive), 12 minutes of EEG with 18 channels recorded at a 2 kHz sampling rate required approximately 1-2 seconds for filtering and rectification; after that, the detection procedure took an additional 2-3 seconds per channel for a single value of α. Overall, it took about 40 seconds to obtain initial detection results when no window segments were applied. After implementing the windowing method, the time needed for initial detection went up to 10 minutes. Calculating the ROC curves with 90 parameter combinations took around 12 hours. Additionally, if the time window is too small, the amplitude distribution of the background activity in one window might not be similar to a gamma distribution, and this would

compromise the optimization of the α parameter. Therefore, an appropriate window size is also important in order to achieve satisfactory results.

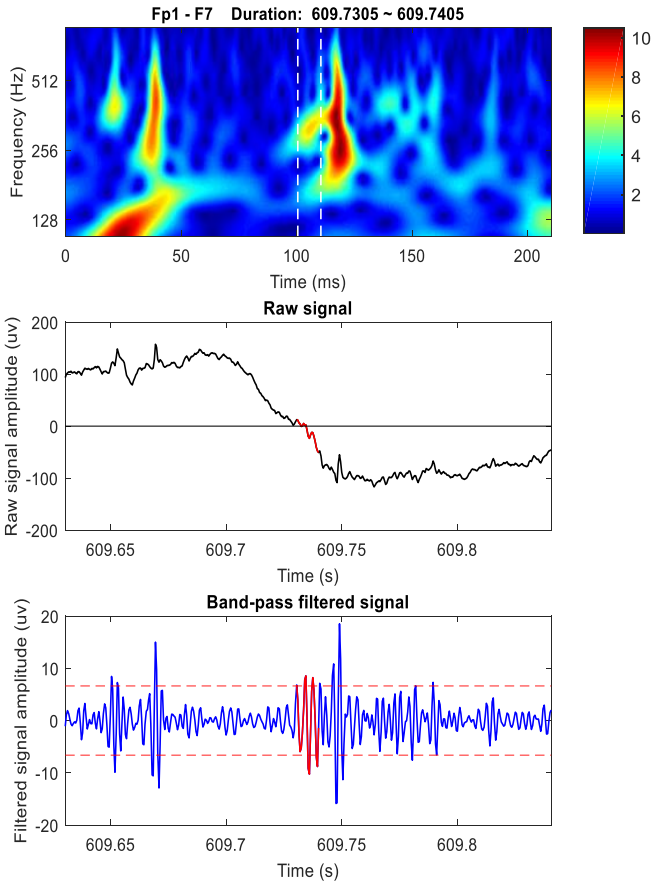

Figure 4.2. Example of a false detection. The signal in red has enough peaks exceeding the threshold, but doesn't stand out from the background. The signal on the right of the red portion seems to stand out, both in filtered data and time-frequency map, but it doesn't have enough peaks over the threshold, and thus was not marked either visually or automatically.

We used two different methods to compare the detection outcome. First, we used ROC curves to measure the best possible performance of each detector. The point on the ROC curve with shortest distance to the upper left corner was regarded as the best balance between TPR and FDR, thus the parameter set associated with that point was defined as the optimum parameter set. Second, to address the practical situation in which visual detection

is not available for all channels, we employed a leave-one-out cross-validation test both within two different groups of patients and across all seven patients. This test was completed independently for each group and assumed that the distribution of automatic detections among channels in different datasets could be categorized into either Group 1 and Group 2. If we want to test the detector performance when applied to a new dataset using this method without prior knowledge of visual markings, we would first examine the distribution of detections across all 18 channels and evaluate the SNR of the dataset. Although detection results using different parameter combinations were distinct, measured as the total number of automatic detections, the relative number of events in each channel was similar. Therefore, we would set a moderate criterion (5 out of 6 peaks with $\alpha = 0.001$) and examine the distribution of detections. If the distribution falls in Group 1 and the dataset has high SNR, the optimized parameter set in the first three datasets will be used. Likewise, the optimum parameter combination in Group 2 will be applied if the test dataset has low SNR.

Overall, our detector had good sensitivity (86.3%) with a low false detection rate (11.3%). These values indicate that only approximately one out of ten detected HFO events occurred outside of the visual markings. Compared with a published fast oscillation automatic detection algorithm applied on scalp EEG data (von Ellenrieder et al., 2011), whose best sensitivity reached 95% with a false detection rate around 40%, our algorithm provides an advantage, especially with the lower number of false positives. In some datasets where HFOs occurred simultaneously in several channels and possible false positive events were visually marked in close proximity to artifacts, the performance of the detector was greatly affected. Another factor that may have influenced the performance is that the detection relies on the identification of local maxima in rectified filtered signals. Thus, the

performance of the detector is highly sensitive to events with high amplitude. So if the pre-defined NPEAKTH value is too low, some short and sharp events with fewer peaks exceeding the threshold are more likely to be marked by the detector. It should also be noted that the detector performance in Group 2 was worse due to the fact that many HFOs didn't stand out from the background. It might also be due to the fact that the consensus among human reviewers in these datasets was low, which means inherent bias existed. This explains why the standard deviation for TPR and FDR is high and the cross-validation results within all seven patients was worse than the test completed in the two groups independently. To solve this problem, the internal consistency of human annotations of these datasets needs to be taken into serious consideration and other post-processing methods should be applied depending on whether high TPR or low FDR is desired under certain specific conditions.

In conclusion, this simple algorithm can be used to automatically detect HFOs with a high degree of accuracy, confirmed by comparison to visually marked events. Since it only requires the optimization of the alpha value (related to the percentage of allowable false positive events) and the number of consecutive peaks, it can be applied consistently across scalp EEG data from different centers. In addition, categorization of datasets according to their detection distribution and the implementation of artifact rejection methods make the detector more powerful because they help distinguish between datasets with significantly different characteristics and decrease false detections. It can also be easily paired with human visual validation if needed. Overall, due to its high detection sensitivity, simple optimization procedure and effective artifact rejection methods, our detector provides advantages in the detection of HFO events. Its objectivity and efficiency in detection

procedures render it powerful and promising in the assessment and localization of epileptic activities in future applications.

References

(1) Siuly. "Analysis and classification of EEG signals." (2012)

(2) Yazdanpour-Naeini, Roshanak. Automatic detection of high frequency oscillations of neural signals in epileptic patients. Diss. Concordia University, 2012.

(3) Bragin A, Engel Jr J, Wilson CL, Fried I, Buzsáki G. High-frequency oscillations in human brain. Hippocampus 1999; 9:137–142.

(4) Jacobs J, Zijlmans M, Zelmann R, Chatillon CE, Hall J, Olivier A, Dubeau F, Gotman J. High-frequency electroencephalographic oscillations correlate with outcome of epilepsy surgery. Ann Neurol 2010; 67:209–220.

(5) Wu JY, Sankar R, Lerner JT, Matsumoto JH, Vinters HV, Mathern GW. Removing interictal fast ripples on electrocorticography linked with seizure freedom in children. Neurology 2010; 75:1686–1694

(6) Bragin A, Wilson CL, Engel J. Chronic epileptogenesis requires development of a network of pathologically interconnected neuron clusters: a hypothesis. Epilepsia 2000;41(suppl 6): S144–S152

(7) Engel Jr, Jerome, et al. "High-frequency oscillations: What is normal and what is not?." Epilepsia 50.4 (2009): 598-604.

(8) López-Cuevas, Armando, et al. "An algorithm for on-line detection of high frequency oscillations related to epilepsy." Computer methods and programs in biomedicine 110.3 (2013): 354-360.

(9) Chaibi, Sahbi, et al. "Automated detection and classification of high frequency oscillations (HFOs) in human intracereberal EEG." Biomedical Signal Processing and Control 8.6 (2013): 927-934.

(10) Zelmann, R., et al. "A comparison between detectors of high frequency oscillations." Clinical Neurophysiology 123.1 (2012): 106-116.

(11) Staba, Richard J., et al. "Quantitative analysis of high-frequency oscillations (80–500 Hz) recorded in human epileptic hippocampus and entorhinal cortex." Journal of neurophysiology 88.4 (2002): 1743-1752.

(12) Gardner, Andrew B., et al. "Human and automated detection of high-frequency oscillations in clinical intracranial EEG recordings." Clinical neurophysiology 118.5 (2007): 1134-1143.

(13) Grange, Wilfried, et al. "Detection of transient events in the presence of background noise." The Journal of Physical Chemistry B 112.23 (2008): 7140-7144.

(14) Gliske, Stephen V., et al. "Universal automated high frequency oscillation detector for real-time, long term EEG." Clinical Neurophysiology 127.2 (2016): 1057-1066.

(15) Amiri, Mina, et al. "High frequency oscillations and spikes: separating real HFOs from false oscillations." Clinical Neurophysiology 127.1 (2016): 187-196.

(16) Abhang, Priyanka A., and Bharti W. Gawali. "Correlation of EEG Images and Speech Signals for Emotion Analysis." British Journal of Applied Science & Technology 10.5 (2015): 1-13.

(17) Worrell, Gregory. "High-frequency oscillations recorded on scalp EEG." Epilepsy currents 12.2 (2012): 57-58.

(18) Höller, Yvonne, et al. "High-frequency oscillations in epilepsy and surgical outcome. A meta-analysis." Frontiers in human neuroscience 9 (2015): 574.

(19) Navarrete, Miguel, et al. "Automated detection of high-frequency oscillations in electrophysiological signals: Methodological advances." Journal of Physiology-Paris (2017).

(20) Navarrete, Miguel, et al. "RIPPLELAB: A Comprehensive Application for the Detection, Analysis and Classification of High Frequency Oscillations in Electroencephalographic Signals." PloS one 11.6 (2016): e0158276.

(21) Liu, Su, et al. "Exploring the time–frequency content of high frequency oscillations for automated identification of seizure onset zone in epilepsy." Journal of neural engineering 13.2 (2016): 026026.

(22) Jrad, Nisrine, et al. "Automatic detection and classification of High Frequency Oscillations in depth-EEG signals." IEEE Transactions on Biomedical Engineering (2016).

(23) Kucewicz, Michal T., et al. "High frequency oscillations are associated with cognitive processing in human recognition memory." Brain (2014): awu149.

(24) Zijlmans, Maeike, et al. "High-frequency oscillations as a new biomarker in epilepsy." Annals of neurology 71.2 (2012): 169-178.

(25) Gliske, Stephen V., et al. "Universal automated high frequency oscillation detector for real-time, long term EEG." Clinical Neurophysiology 127.2 (2016): 1057-1066.

(26) Fedele, Tommaso, et al. "Automatic detection of high frequency oscillations during epilepsy surgery predicts seizure outcome." Clinical Neurophysiology 127.9 (2016): 3066-3074.

(27) Zelmann, R., et al. "Scalp EEG is not a blur: it can see high frequency oscillations although their generators are small." Brain topography 27.5 (2014): 683-704.

(28) Burnos, Sergey, et al. "Human intracranial high frequency oscillations (HFOs) detected by automatic time-frequency analysis." PLoS One 9.4 (2014): e94381.

(29) Burnos, Sergey, et al. "The morphology of high frequency oscillations (HFO) does not improve delineating the epileptogenic zone." Clinical Neurophysiology 127.4 (2016): 2140-2148.

(30) Melani, Federico, et al. "Occurrence of scalp-fast oscillations among patients with different spiking rate and their role as epileptogenicity marker." Epilepsy research 106.3 (2013): 345-356.

(31) Andrade-Valenca, L. P., et al. "Interictal scalp fast oscillations as a marker of the seizure onset zone." Neurology 77.6 (2011): 524-531.

(32) Pizzo, Francesca, et al. "Detectability of fast ripples (> 250 hz) on the scalp EEG: a proof-of-principle study with subdermal electrodes." Brain topography 29.3 (2016): 358-367.

(33) von Ellenrieder, Nicolás, et al. "Automatic detection of fast oscillations (40–200Hz) in scalp EEG recordings." Clinical Neurophysiology 123.4 (2012): 670-680.

(34) Jacobs, J., et al. "High-frequency oscillations (HFOs) in clinical epilepsy." Progress in neurobiology 98.3 (2012): 302-315.

(35) Worrell, Gregory Alan, et al. "Recording and analysis techniques for high-frequency oscillations." Progress in neurobiology 98.3 (2012): 265-278.

(36) Engel, Jerome, and Fernando Lopes da Silva. "High-frequency oscillations–where we are and where we need to go." Progress in neurobiology 98.3 (2012): 316-318.

(37) Urrestarazu, Elena, et al. "Interictal high-frequency oscillations (100–500 Hz) in the intracerebral EEG of epileptic patients." Brain 130.9 (2007): 2354-2366.

(38) Cosandier-Rimélé, Délphine, et al. "Recording of fast activity at the onset of partial seizures: depth EEG vs. scalp EEG." Neuroimage 59.4 (2012): 3474-3487.

(39) Iwatani, Yoshiko, et al. "Ictal high-frequency oscillations on scalp EEG recordings in symptomatic West syndrome." Epilepsy research 102.1 (2012): 60-70.

(40) Kobayashi, Katsuhiro, et al. "A storm of fast (40–150Hz) oscillations during hypsarrhythmia in West syndrome." Annals of neurology 77.1 (2015): 58-67.

(41) von Ellenrieder, Nicolás, et al. "Size of cortical generators of epileptic interictal events and visibility on scalp EEG." Neuroimage 94 (2014): 47-54.

(42) Jasper, Herbert Henri. Jasper's basic mechanisms of the epilepsies. Vol. 80. OUP USA, 2012.